DEPARTMENT OF COMMERCE
LUTHER H. HODGES, Secretary

WEATHER BUREAU
F. W. REICHELDERFER, Chief

MONTHLY WEATHER REVIEW

JAMES E. CASKEY, JR., Editor

Volume 89
Number 6

JUNE 1961

Closed May 15, 1961
Issued June 15, 1961

COMPUTATION AND USES OF GRADIENT WINDS

ROY M. ENDLICH

Stanford Research Institute, Menlo Park, Calif.
[Manuscript received December 13, 1960; revised March 6, 1961]

ABSTRACT

The viewpoint is taken that in large portions of the atmosphere, wind speeds (V_{gr}), divergence (D_{gr}), and vorticity (ζ_{gr}) obtained under the gradient wind assumption are considerably more accurate representations of true conditions than those one obtains from the geostrophic assumption. Equations are derived for computing V_{gr}, D_{gr}, and ζ_{gr}. The equation for the vorticity of gradient winds has a considerable resemblance to "balance" equations of Charney [3] and Phillips [17]. Gradient winds and their space derivatives may have advantages over other formulations due to their relative simplicity. The quantities V_{gr}, D_{gr}, and ζ_{gr} may be computed quite easily from geopotential data at grid points by use of high-speed computers. Possible applications of gradient winds in practical and theoretical meteorology are suggested.

1. INTRODUCTION

The geostrophic wind equation, an empirical relation which equates horizontal pressure and Coriolis forces, is a well-known cornerstone of both theoretical and applied meteorology in extratropical latitudes. One might expect that a generalization of the geostrophic equation to include a third term of major importance, namely, the centrifugal force, would lead to more accurate modeling of winds than the simple geostrophic relation provides. However, the reader will immediately realize that the centrifugal force V^2K, where V is wind speed and K is the trajectory curvature, is small in regions of weak winds, and that in regions of straight flow the gradient wind automatically degenerates into the geostrophic. For example, Neiburger et al. [13] compared geostrophic and gradient winds with observed winds on two 700-mb. charts having a mean observed speed of 18 kt. and found that gradient winds were not significantly better than geostrophic. In a study of strong winds (having an average speed of 94 kt.), Endlich and McLean [7] found that in cyclonically-curved jet streams, geostrophic winds overestimated wind speeds measured by aircraft by 28 kt. on the average (18 percent of the geostrophic speeds of the sample) while gradient winds differed only minutely from measured values. In other words, the centrifugal force was 18 percent of the pressure force. The standard deviation of geostrophic departures (after accounting for observational errors) was estimated as 22 kt. while the standard deviation of gradient departures was estimated as 5.5 kt. From these data, one would conclude that in and around jet streams, and probably also in relatively strong currents at other altitudes, consideration of the centrifugal force accounts for the major part of the ageostrophic components. Remaining ageostrophic components are due to cross-contour flow, to vertical motions, and to friction. However, studies of constant-level balloon trajectories (Neiburger and Angell [12], Angell [1]) indicate that cross-contour components are relatively large, being on the average about two-thirds of the magnitude of the along-contour (centrifugal) components. Thus, the question of the relative magnitude of the two

ageostrophic components is presently unresolved. Nevertheless, Angell estimates that the percentage error in estimating winds geostrophically exceeds 29 percent half of the time, while the error of the gradient assumption is considerably less, exceeding 11 percent half of the time. In practice, one can include the centrifugal components by use of gradient winds; however, the cross-contour components, though important in initiating disturbances and in subsynoptic phenomena, are very difficult to estimate from conventional data.

The hypothesis is therefore proposed that gradient winds provide an estimate of actual winds which is sufficiently accurate to make them useful in describing the dynamics of synoptic-scale processes. In support of this hypothesis, one may recall that the propagation of cyclone waves was explained (see, for example, the review by Bjerknes [2]) on the basis of divergence of gradient winds in advance of upper-level troughs and convergence behind. Moreover, Phillips [17] has shown that strictly non-divergent winds introduce "meteorological noise" and are not suitable for computing initial data for numerical prediction based on integration of the primitive equations. Gradient winds, which are divergent yet approximately geostrophic, might provide a simple, relatively noiseless balance condition between winds and the geopotential field. It will be shown later that the equation for gradient vorticity (ζ_{gr}) is quite similar to the well-known balance equation (Petterssen [14], Charney [3]) and to a vorticity equation based on a divergent wind (Edelmann [6], Phillips [17]).

One of the main difficulties to be expected in computing winds (and especially divergence fields) from present upper-air data is that random errors caused by observational inaccuracies will be contained in the results. Therefore, smoothing of computed values may be a prerequisite to their use.

In order to determine whether advantages accrue, in practice, from the explicit calculation of gradient winds and their divergence and vorticity fields, in the future it will be necessary to carry out computations for comparison with observed winds and with divergence and vorticity calculated by other techniques. In the present article, a simple method of successive approximations is developed for computing V_{gr}, D_{gr}, and ζ_{gr}. The nature of the computational scheme is such that it can be carried out quite simply and rapidly by use of electronic computers.

2. COMPUTATION OF VELOCITY, DIVERGENCE, AND VORTICITY OF GRADIENT FLOW

The basic assumptions of gradient flow (e.g., Holmboe et al. [11]) are that air parcels maintain constant speed (i.e., do not cross the contours on constant pressure charts toward higher or lower heights) and move horizontally and without friction. The equation which results on introduction of these assumptions into the horizontal equation of motion may be written as follows:

$$V_{gr}^2\,(d\theta/ds)\,\mathbf{n}=-f(V_{gr}-V_g)\,\mathbf{n} \tag{1}$$

where V_{gr} is the gradient speed; θ is the wind direction taken as positive in the counter-clockwise direction; s is distance along the path; $d\theta/ds$ is K the curvature of the path; $\mathbf{n}=-\nabla\phi/|\nabla\phi|$ is a unit vector directed to the left of the path, ∇ operates at constant pressure, and $\phi=gz$; f is the Coriolis parameter; and V_g is the geostrophic wind speed. The term on the left side represents the centrifugal force which is proportional to the difference between V_{gr} and V_g.

If we post-multiply equation (1) vectorially by the vertical unit vector $\mathbf{k}$ we obtain

$$f\mathbf{V}_{gr}=f\mathbf{V}_g-V_{gr}^2\,(d\theta/ds)(\mathbf{n}\times\mathbf{k}). \tag{2}$$

Also
$$f\mathbf{V}_g=\mathbf{k}\times\nabla\phi=|\nabla\phi\,(\mathbf{n}\times\mathbf{k}) \tag{3}$$

or
$$\mathbf{n}\times\mathbf{k}=(1/|\nabla\phi|)f\mathbf{V}_g.$$

Therefore
$$\mathbf{V}_{gr}=[1-(V_{gr}^2/|\nabla\phi|)(d\theta/ds)]\mathbf{V}_g. \tag{4}$$

After a further simplification, this form of the gradient wind equation will be used to compute V_{gr}. The simplification involves the use of Blaton's formula

$$\frac{d\theta}{ds}=\frac{dt}{ds}\frac{d\theta}{dt}=\frac{1}{V}\left(\frac{\partial\theta}{\partial t}+V\frac{\partial\theta}{\partial s}+\omega\frac{\partial\theta}{\partial p}\right)\approx\frac{1}{V}\frac{\partial\theta}{\partial t}+\frac{\partial\theta}{\partial s} \tag{5}$$

i.e., we neglect the term containing the vertical advection of θ. If vertical motion is present, actual three-dimensional trajectories tend to be less cyclonic than trajectories estimated on isobaric charts (Danielsen [5]). The difference is greatest in fronts or other phenomena where vertical motions reach maximum values. It is of lesser, and perhaps negligible, importance in larger-scale motions. As there is no simple method for estimating the magnitude of the difference, it will be neglected in the remainder of this paper.

We will now define a parameter $k=(1/|\nabla\phi|)(d\theta/ds)$ or from equation (5)

$$k=(1/|\nabla\phi|)(\partial\theta/\partial s)+(1/|\nabla\phi|)(1/V)(\partial\theta/\partial t) \tag{6}$$

where k represents the trajectory curvature, the first term on the right measures the contour curvature, and the second term measures the local change in wind direction. For cyclonic trajectories $k>0$ and for anticyclonic, $k<0$. Since we have assumed flow parallel to contours, $\partial\theta/\partial t$ may be evaluated as the local change in contour direction. This direction may be measured counterclockwise from east so that

$$\theta=\tan^{-1}(v_g/u_g)=\tan^{-1}(-\phi_x/\phi_y) \tag{7}$$

where the subscripts x and y denote partial derivatives eastward and northward.

To evaluate equation (6) we use $\partial\theta/\partial s=\cos\theta(\partial\theta/\partial x)+\sin\theta(\partial\theta/\partial y)$ where θ is given by equation (7) and, as a matter of convenience, substitute V_g for V. Then

$$k=(\phi_x^2+\phi_y^2)^{-2}[(\phi_y^2\phi_{xx}-2\phi_x\phi_y\phi_{xy}+\phi_x^2\phi_{yy})+f(\phi_x\phi_{yt}-\phi_y\phi_{xt})]. \quad (8)$$

Given the distribution of ϕ at grid points on a constant pressure chart, one can easily compute a finite difference approximation to the first term in the bracket. A shortened version of this term has been used by Phillips [16] in computing contour curvature. The second term in the bracket can be evaluated as the difference between geopotential gradients on charts separated in time, or from the space variations of geopotential tendency.

For progressive, wave-shaped contour patterns, the curvatures of trajectories and contours are of the same sign (unless the waves are traveling faster than the winds); however, the trajectories are less sharply curved than the contours.[1] In other words, the term $(1/V)(\partial\theta/\partial t)$ is generally of opposite sign but smaller magnitude than $\partial\theta/\partial s$. The smoothing effect of a finite-difference evaluation of $\partial\theta/\partial s$ tends to reduce its magnitude toward the magnitude of the trajectory curvature. Therefore, on upper-level charts, especially where V is large, it may prove feasible to neglect the term containing $(1/V)(\partial\theta/\partial t)$.

Having obtained a value of k at each grid point by use of equation (8), we may write equation (4) in vector or scalar form as

$$\mathbf{V}_{gr}=(1-kV_{gr}^2)\mathbf{V}_g \text{ or } V_{gr}=(1-kV_{gr}^2)V_g. \quad (9)$$

This quadratic equation may be solved for V_{gr} since k and V_g are known. In the past, the solution has ordinarily been obtained graphically; e.g., Gustafson [9]. If the equation is solved by electronic computer, the square root in the quadratic formula is calculated by use of an initial guess and successive approximations. It appears that a solution to equation (9) may be obtained more directly and simply by the following process of successive approximations. As a first guess, we may substitute V_g^2 for V_{gr}^2 on the right side of (9). Then if we replace the subscript on V_{gr} by the number of the approximation we obtain

$$\begin{aligned} V_1&=(1-kV_g^2)V_g \\ V_2&=(1-kV_1^2)V_g \\ &\cdots \\ V_n&=(1-kV_{n-1}^2)V_g. \end{aligned} \quad (10)$$

The convergence of V_n to V_{gr} is quite rapid as shown in figure 1. Here we have assumed a typical jet stream condition where $V_g=125$ kt. and $k=2\times10^{-5}$ kt.$^{-2}$ (cyclonic curvature) so that $V_{gr}=100$ kt. The approximations fall alternately on opposite sides of V_{gr} and in this particular case, V_5 approaches V_{gr} within 1 percent. For

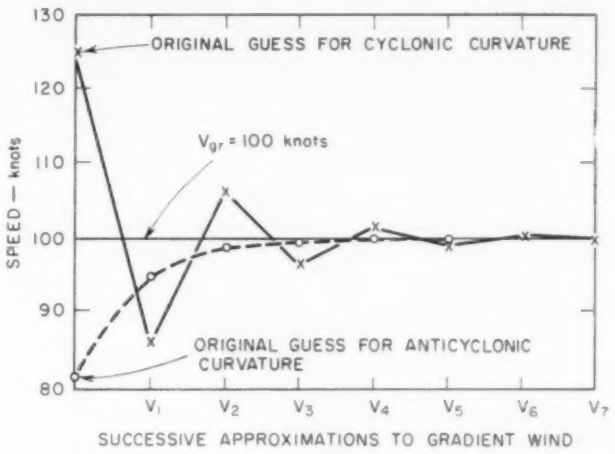

FIGURE 1.—Graph showing the convergence of successive approximations to true gradient wind speed (V_{gr}) using the geostrophic speed (V_g) as the initial guess. Solid lines join approximation for cyclonic curvature; dashed curve joins approximations for anticyclonic curvature. Approximations computed using equation (10) in text.

$V_g=83.3$ and $k=-2\times10^{-5}$ (anticyclonic curvature), the approximations approach V_{gr} asymptotically. In this example, V_3 approached V_{gr} (100 kt.) within 1 percent. It can be shown that for these two examples, convergence will occur if the absolute value of the initial guess is less than 500 kt. In general, the region of convergence is quite broad. The geostrophic speed is a convenient initial guess which is in the neighborhood of the gradient speed and therefore results in an acceptable estimate of the gradient speed after a small number of successive approximations.

For anticyclonic flow and for a given radius of curvature, V_{gr} increases with V_g up to a limit of $2V_g$. Beyond this point, the quantity $4kV_g^2<-1$ and equation (9) has complex solutions which have no physical reality. Gradient wind balance does not exist in these "unstable ridges" and the approximations of equation (10) will not converge. Grid points at which this equation diverges may be marked with a special symbol to indicate the absence of gradient flow. Unstable ridges, though rather uncommon, are synoptically important since cut-off Lows sometimes form downstream (Bjerknes [2]).

We will assume that by using equation (10) we have obtained a satisfactory estimate of V_{gr} at each grid point (with the exceptions mentioned above). Now it is convenient to define a quantity

$$B=-kV_{gr}^2$$

so that equation (9) becomes

$$V_{gr}=(1+B)V_g \text{ or } B=(V_{gr}-V_g)/V_g. \quad (11)$$

B is a non-dimensional term which expresses the departure

[1] The relationships between streamlines and trajectories are discussed by Holmboe et al. [11] and Haltiner and Martin [10], among others.

of the gradient speed from the geostrophic as a fraction of the geostrophic speed. It may also be thought of as the correction to be made to the geostrophic wind in order to obtain the gradient wind. For convenience, it will be referred to as the "gradient correction." In a roughly sinusoidal pattern of contours in which a jet stream is imbedded, one would expect centers of negative B with central values of about 20 percent where the jet crosses troughs, and similar centers of positive B where the jet crosses ridges.

The "gradient divergence" is defined as

$$D_{gr}=\nabla\cdot\mathbf{V}_{gr}=\nabla\cdot(1+B)\mathbf{V}_g=\mathbf{V}_g\cdot\nabla B+(1+B)\nabla\cdot\mathbf{V}_g. \quad (12)$$

The divergence therefore depends on the geostrophic wind and the field of the gradient correction B. To obtain a quantitative estimate of the first term on the right side of equation (12), we take a typical value of geostrophic wind speed as 30 m. sec.$^{-1}$ To obtain a typical value of ∇B, we assume that B changes from -0.20 in a trough to zero at an inflection point over a distance of 600 km. Then $\mathbf{V}_g\cdot\nabla B$ equals 10^{-5} sec.$^{-1}$ The second term on the right side of (12) is generally an order of magnitude smaller but may be of importance in strong meridional currents in middle or low latitudes. Therefore $D_{gr}\sim10^{-5}$ sec.$^{-1}$ which is of the order expected for progressive waves.

The relative vorticity of the gradient wind at any point is

$$\zeta_{gr}=\mathbf{k}\cdot\nabla\times\mathbf{V}_{gr}=(1+B)\zeta_g+\mathbf{k}\cdot\nabla B\times\mathbf{V}_g \quad (13)$$

where $\zeta_g=\mathbf{k}\cdot\nabla\times\mathbf{V}_g$ is the geostrophic vorticity. Since B is negative in cyclonic flow and positive in anticyclonic, the term $(1+B)$ on the right side of (13) tends to make ζ_{gr} either less or more than ζ_g. Petterssen [14] has shown that the geostrophic vorticity overestimates the vorticity of cyclones and underestimates it in anticyclones. Therefore, B provides a correction in the proper direction.

Letting $\beta=\partial f/\partial y$ and using equation (3), $\zeta_g=f^{-1}(\nabla^2\phi+\beta u_g)$. On expansion, the last term in (13) is $v_gB_x-u_gB_y$. Using these relations, equation (13) becomes

$$(1+B)\nabla^2\phi-f\zeta_{gr}+(1+B)\beta u_g+fv_gB_x-fu_gB_y=0. \quad (14)$$

In a machine computation of gradient winds and their divergence and vorticity, one might proceed as follows:

1. Tabulate the geopotential at grid points on a constant pressure chart.

2. Using geopotential data at neighboring grid points as finite-difference approximations to partial derivatives, compute u_g, v_g, and V_g (equation (3)), and θ (equation (7)).

3. The curvature parameter k (equation (8)) may be computed in two steps. Compute the first term in the bracket from the grid point data of step 2. The second term in the bracket may be computed as the difference between past and present values of ϕ_x and ϕ_y or as the eastward and northward changes in geopotential tendency.

4. At each grid point, compute V_{gr} from V_g and k (equation (10)).

5. Compute B at each point from V_{gr} and V_g (equation (11)).

6. Approximate ∇B by finite differences and compute D_{gr} at each point (equation (12)). If desired, vertical motions may be obtained from D_{gr} by use of the continuity equation with appropriate boundary conditions.

7. Compute ζ_{gr} from equation (13) or (14).

It should be noted that these calculations do not require solution of first or second order operators over the grid. A rough estimate indicates that all of the above quantities (except vertical motion) can be calculated by a high-speed computer such as the IBM 704, for a 2000-point grid in approximately 30 seconds.

3. COMPARISON OF THE VORTICITY OF GRADIENT WINDS WITH OTHER BALANCE RELATIONS

Equation (14) bears a strong resemblance in its first three terms to corresponding terms in the "balance" equation (Petterssen [14], Charney [3]) written as

$$\nabla^2\phi-f\zeta+\beta u+u_x^2+2v_xu_y+v_y^2=0 \quad (15a)$$

or in terms of a streamfunction as

$$\nabla^2\phi-f\nabla^2\psi-\beta\psi_y-2(\psi_{xx}\psi_{yy}-\psi_{xy}^2)=0. \quad (15b)$$

A slightly different equation has been obtained by Edelmann [6] and Phillips [17]:

$$\nabla^2\phi-f\zeta+\beta u_g-2f^{-2}(\phi_{xx}\phi_{yy}-\phi_{xy}^2)=0. \quad (16)$$

It should be noted that the vorticity specified by this equation generally differs somewhat from that given by equation (15).

The similarities of equations (14), (15), and (16) are evidently due to the fact that they are all obtained from the horizontal equation of motion by approximating the acceleration in one way or another. The gradient wind approximates $d\mathbf{V}/dt$ by the centrifugal force and is equivalent to expressing the geostrophic departure $\mathbf{V}'$ as

$$\mathbf{V}'=\mathbf{V}-\mathbf{V}_g\approx\mathbf{V}_{gr}-\mathbf{V}_g=f^{-1}(\mathbf{k}\times\mathbf{n})V_{gr}^2\,(d\theta/ds). \quad (17)$$

As mentioned earlier, equation (14) is simply the vorticity of the gradient wind. Equation (15) is obtained by taking the divergence of the horizontal equation of motion and then neglecting the terms $d(\nabla\cdot\mathbf{V})/dt$ and $\nabla\omega\cdot(\partial\mathbf{V}/\partial p)$. The wind field specified by this equation is non-geostrophic and non-divergent. Equation (16) gives the vorticity of a divergent, quasi-geostrophic wind which is obtained by expressing the geostrophic departure $\mathbf{V}'$ as $f^{-1}\,\mathbf{k}\times(d\mathbf{V}/dt)$ and by approximating $d\mathbf{V}/dt$ geostrophically (Philipps [15]) so that

$$\mathbf{V}'=f^{-1}\mathbf{k}\times(\partial\mathbf{V}_g/\partial t+\mathbf{V}_g\cdot\nabla\mathbf{V}_g). \quad (18)$$

As a consequence of his demonstration that non-divergent initial wind fields introduce "meteorological noise" into integrations of the primitive equations, Phillips [17] has proposed obtaining initial wind data by solution of three simultaneous equations (not repeated here) which give D, the horizontal divergence. ζ is determined from equation (16), and D and ζ with boundary conditions determine a wind field which is relatively "noiseless."

In the writer's opinion, the relative merits of expressing $\mathbf{V}'$ by equation (17) or by equation (18) are difficult to judge on theoretical grounds. It follows that equations (14) and (16) are equally plausible; however, gradient winds and their divergence and vorticity appear much simpler to compute than the comparable quasi-geostrophic, divergent quantities. It may be logical, therefore, to compute ζ_{gr}, $\nabla^2\psi$, and ζ by using equations (14), (15), and (16), respectively, from actual data for a number of cases. The three vorticity (or corresponding wind) fields might then be compared and tested in actual forecasts.

4. APPLICATIONS OF GRADIENT WINDS

The following applications of gradient winds appear to warrant further investigation:

1. Specifying winds on current or forecast charts. Gradient winds might be used in flight forecasting for aircraft, in determining trajectories, and in locating jet streams (Endlich and McLean [8]) and fronts.

2. Use as a balance condition between winds and the geopotential field; for example, in computing initial vorticity fields for use in forecasting with the vorticity equation or in computing initial wind data for use in integrations of the primitive equations.

3. Determination of a first approximation to horizontal divergence fields and corresponding vertical motions.

4. As a means of introducing wind data into the objective analysis of fields of geopotential or streamfunction in place of the current "geostrophic" use of observed winds (Cressman [4]). A possible method of introducing observed winds according to the gradient assumption would be to compute the gradient correction (B) that corresponds to the geopotential field used as the initial guess. Observed winds divided by $(1+B)$ would give geostrophic winds for use in the objective analysis procedure.

As mentioned in the Introduction, the application of gradient winds to the problems mentioned above is based on the empirically supported hypothesis that they provide a considerably more accurate approximation to true conditions than the more restrictive geostrophic assumption provides; however, this hypothesis must be tested further with observational data before a final judgment of its validity can be made.

ACKNOWLEDGMENT

The writer is indebted to Dr. Manfred M. Holl for a number of helpful suggestions given during the course of this study.

REFERENCES

1. J. K. Angell, "Some Statistics on the Magnitude of the Ageostrophic Wind Obtained from Constant Level Balloon Data," *Monthly Weather Review*, vol. 87, No. 5, May 1959, pp. 163–170.
2. J. Bjerknes, "Extratropical Cyclones," *Compendium of Meteorology*, American Meteorological Society, Boston, Mass., 1951, pp. 577–598.
3. J. Charney, "The Use of the Primitive Equation of Motion in Numerical Prediction," *Tellus*, vol. 7, No. 1, Feb. 1955, pp. 22–26.
4. G. P. Cressman, "An Operational Objective Analysis System," *Monthly Weather Review*, vol. 87, No. 10, Oct. 1959, pp. 367–374.
5. E. F. Danielsen, "Trajectories: Isobaric, Isentropic, and Actual." (To be published.)
6. W. Edelmann, "Comparison of Different Non-Geostrophic Models with the Aid of Solutions of the Linearized Model Equations," Section F in *Studies in Numerical Weather Forecasting*, Final report under Contract AF61 (514)–735C, Deutscher Wetterdienst, June 30, 1957.
7. R. M. Endlich and G. S. McLean, "Geostrophic and Gradient Departures in Jet Streams," *Journal of Meteorology*, vol. 17, No. 2, Apr. 1960, pp. 135–147.
8. R. M. Endlich and G. S. McLean, "Analyzing and Forecasting Meteorological Conditions in the Upper Troposphere and Lower Stratosphere," *Air Force Surveys in Geophysics*, No. 121, April 1960, Bedford, Mass., 35 pp.
9. A. F. Gustafson, "Theory and Design of a Gradient Wind Scale," Air Weather Service *Technical Report* 105–69, Washington, D.C., 1950.
10. G. J. Haltiner and F. L. Martin, *Dynamical and Physical Meteorology*, McGraw-Hill Book Co., Inc., New York, 1957, 470 pp.
11. J. Holmboe, G. E. Forsythe, and W. Gustin, *Dynamic Meteorology*, John Wiley and Sons, New York, 1945, 378 pp.
12. M. Neiburger and J. K. Angell, "Meteorological Applications of Constant-Pressure Balloon Trajectories," *Journal of Meteorology*, vol. 13, No. 2, Apr. 1956, pp. 166–194.
13. M. Neiburger, L. Sherman, W. W. Kellogg, and A. F. Gustafson, "On the Computation of Wind from Pressure Data," *Journal of Meteorology*, vol. 5, No. 3, June 1948, pp. 87–92.
14. S. Petterssen, "On the Relation between Vorticity, Deformation, and Divergence and the Configuration of the Pressure Field," *Tellus*, vol. 5, No. 3, Aug. 1953, pp. 231–237.
15. H. Philipps, "Die Abweichung vom Geostrophischen Wind," *Meteorologische Zeitschrift*, vol. 56, 1939, pp. 460–483.
16. N. A. Phillips, "Geostrophic Errors in Predicting the Appalachian Storm of November 1950," *Geophysica*, vol. 6, No. 3–4, 1958, pp. 389–405.
17. N. A. Phillips, "On the Problem of Initial Data for the Primitive Equations," *Tellus*, vol. 12, No. 2, May 1960, pp. 121–126.

GRAPHICAL SOLUTION OF THE PENMAN EQUATION FOR POTENTIAL EVAPOTRANSPIRATION

JOHN C. PURVIS

Weather Bureau Airport Station, Columbia, S.C.

[Manuscript received September 8, 1959; revised January 3, 1961]

ABSTRACT

A practicable solution of the Penman formula for potential evapotranspiration by use of graphs is presented. For ease in computation, three graphs are used. These graphs, designed for Columbia, S.C., can be adapted for any location by relabeling or correcting two of the families of curves.

1. INTRODUCTION

Potential evapotranspiration is a measure of the maximum possible water loss from an area under a specified set of weather conditions. This phenomenon may be defined as the water loss from a vegetated surface which is supplied with adequate water at all times. Penman [1] has shown that by the simultaneous solution of a Dalton-type equation and the energy-balance equation one can obtain a fairly simple, yet reasonably sound, equation for estimating potential evapotranspiration. The general form of the Penman equation is

$$E_t=\frac{K(Q_nD+FE_a)}{D+F} \tag{1}$$

where E_t is potential evapotranspiration; D is slope of the saturation vapor pressure vs. temperature curve at the air temperature; F is a constant (we use 0.27) in the equation $R=F\,(T_s-T_a)/(e_s-e_a)$, where R is the Bowen ratio; Q_n is net radiant energy exchange in the same units as the evaporation; E_a is evaporation estimated by a simple equation of the Dalton type; T_s is temperature of the water surface; T_a is temperature of the air; e_s is saturation vapor pressure at the temperature of the water surface; e_a is vapor pressure of the air above the water; and K is a factor applied to account for the difference between open water and a vegetated surface evaporation (Penman suggests 0.6 to 0.8 depending on the season; for the sake of simplicity, we use 0.7).

The evaluation of the Penman formula, equation (1), involves estimating or measuring the energy received by a surface. Because it is presumed, in the Penman approach, that the distribution of energy takes place according to the so-called Bowen ratio, no decision has to be made as to transfer of sensible heat to the water surface.

Rijkoort [2] and van der Bijl [3] present nomographs for the solution of the Penman equation. This paper describes a simpler graphical solution than van der Bijl's nomographs.

2. GRAPHICAL SOLUTION

The equation first derived by Penman [1] is used here with some modification. Units are converted so that the formula will yield estimates of potential evapotranspiration in units of inches of water. For the purpose of these computations, the latent heat of vaporization is computed for approximately the average temperature observed during the summer in South Carolina. Q_n in equation (1) is given by

$$Q_n=R_a(1-r)(0.18+0.55n/N) \\ -ST_a^4(0.56-.092\sqrt{e_a})(0.10+0.90n/N) \tag{2}$$

where R_a is mean monthly extraterrestrial radiation in mm. day^{-1} (evaporation equivalent); r is reflection coefficient, used as 0.05 in Penman formula; n/N is ratio of duration of actual sunshine to maximum possible sunshine; S is Boltzman's constant$=2.01\times10^{-9}$ mm. day^{-1} (evaporation equivalent); T_a is air temperature in F.°; and e_a is actual vapor pressure of air in mm. Hg.

E_a in equation (1) is estimated from a Dalton-type equation:

$$E_a=0.35(e_s-e_a)(0.5+.0098\,u_2) \tag{3}$$

where e_s is saturation vapor pressure of the air in mm. Hg.; e_a is actual vapor pressure of air in mm. Hg.; u_2 is wind speed at 2 m. in miles per day; and E_a is in units of mm. day^{-1}. The constant 0.5 is used in lieu of the constant 1 that Penman used in 1948.

By substitution of (2) and (3) into (1) and conversion of units so that the formula yields inches instead of millimeters of water, the Penman equation becomes [4]

$$E_t=\frac{(.7)(.0394)}{D+.27}DR_a(1-r)(.18+.55\,n/N) \\ +(.27)(.35)(e_s-e_a)(.5+.0098\,u_2)\frac{(.7)(.0394)}{D+.27} \\ -\frac{D(.7)(.0394)}{D+.27}ST_a^4(.56-.092\sqrt{e_a})(.10+.90\,n/N). \tag{4}$$

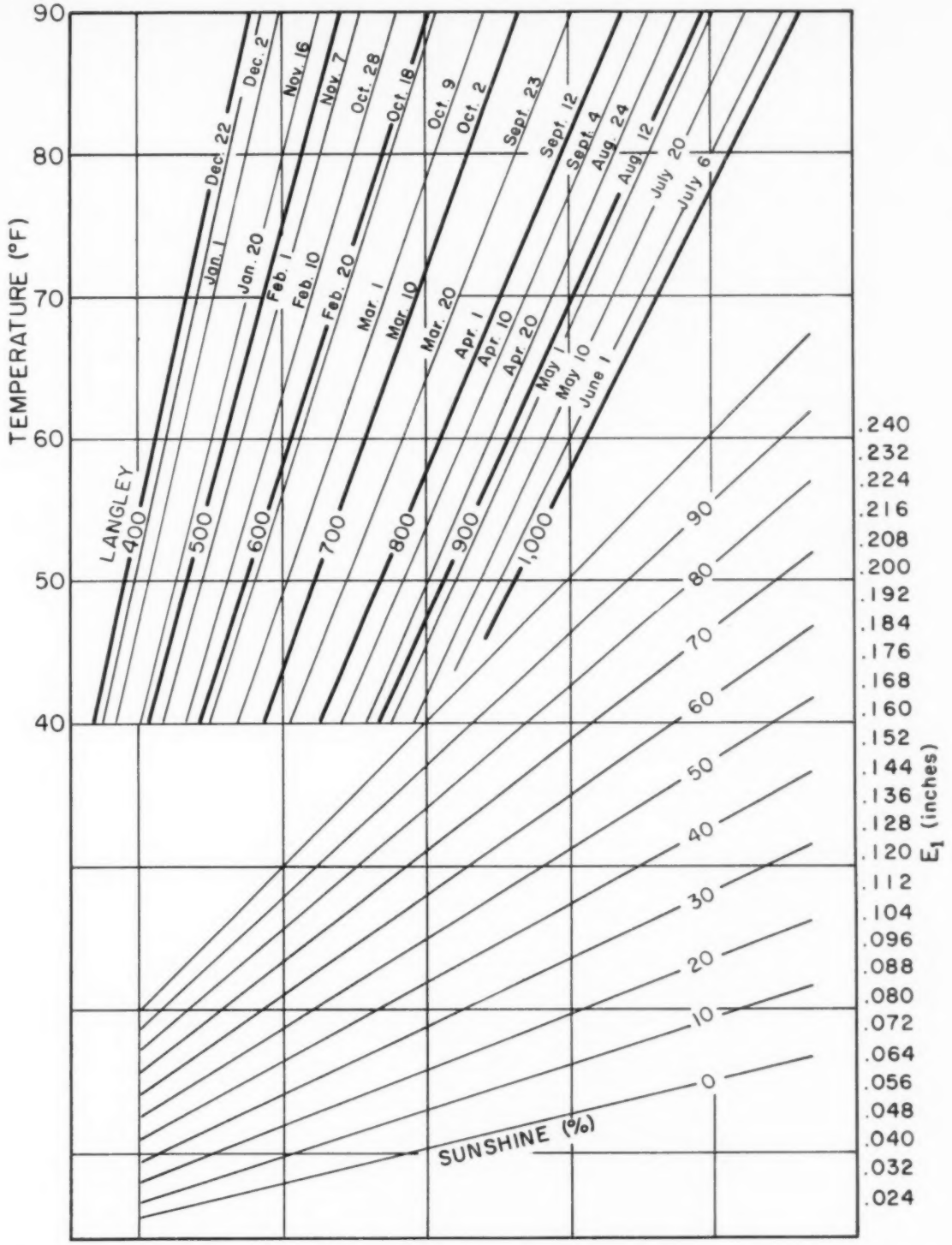

FIGURE 1.—First of three graphs for computation of potential evapotranspiration by Penman formula. This graph yields E_1 as given by equation (6). To use the graph, (1) enter temperature on the upper left scale, (2) move horizontally to the radiation value or calendar date, (3) descend vertically to sunshine percentage, and (4) move horizontally and read value of E_1 on the lower right scale. Dates shown on this graph are for Columbia, S.C.

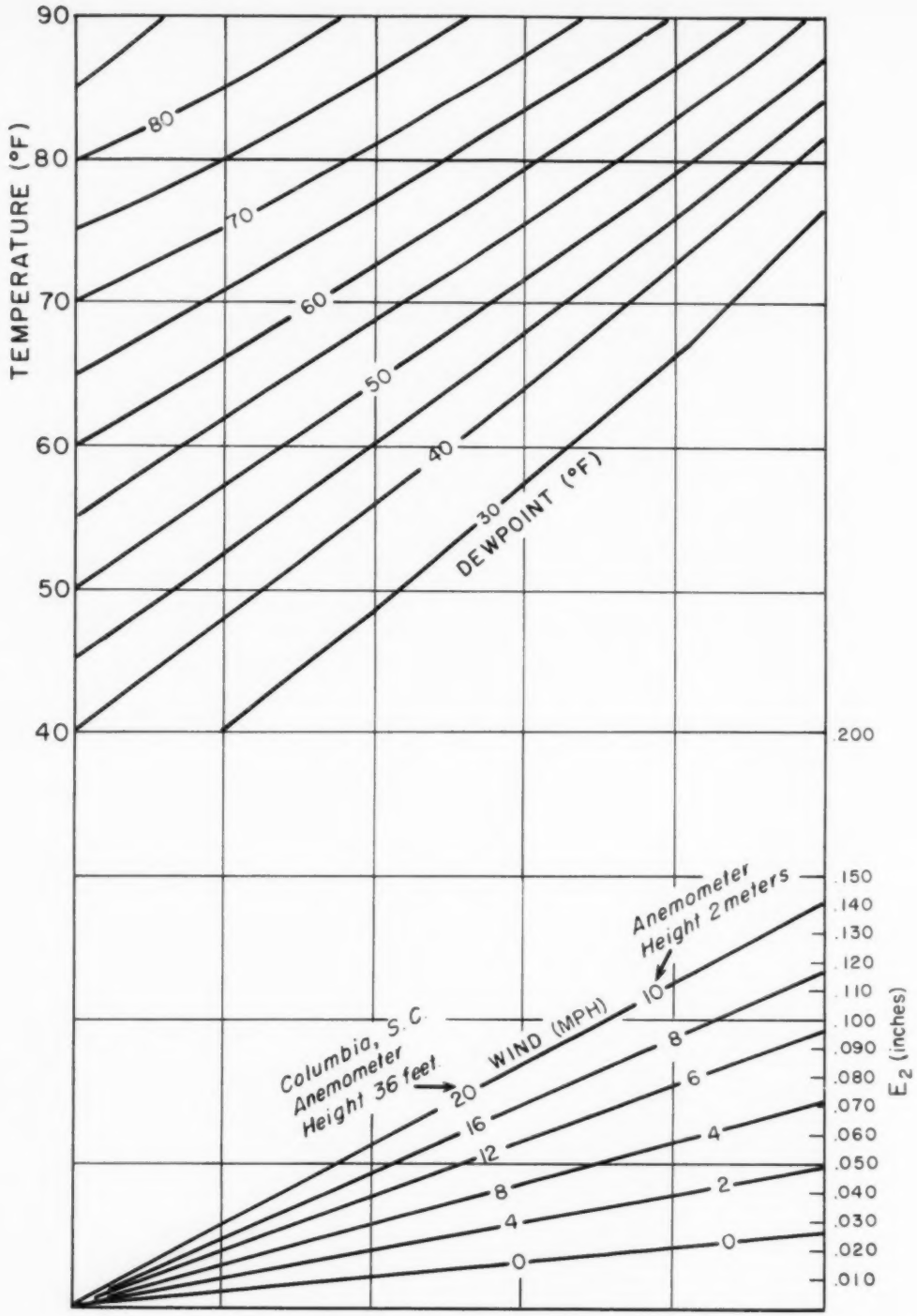

FIGURE 2.—Second of three graphs for computation of potential evapotranspiration by Penman formula. This graph yields E_2 as given by equation (7). To use this graph, enter temperature on the upper left scale, (2) move horizontally to the dew point (average), (3) descend vertically to the wind speed (daily average), and (4) move horizontally and read value of E_2 on the lower right scale. Wind speeds for the Columbia, S.C., anemometer (36-ft. height) are shown to the left of those for an anemometer at 2-m. height.

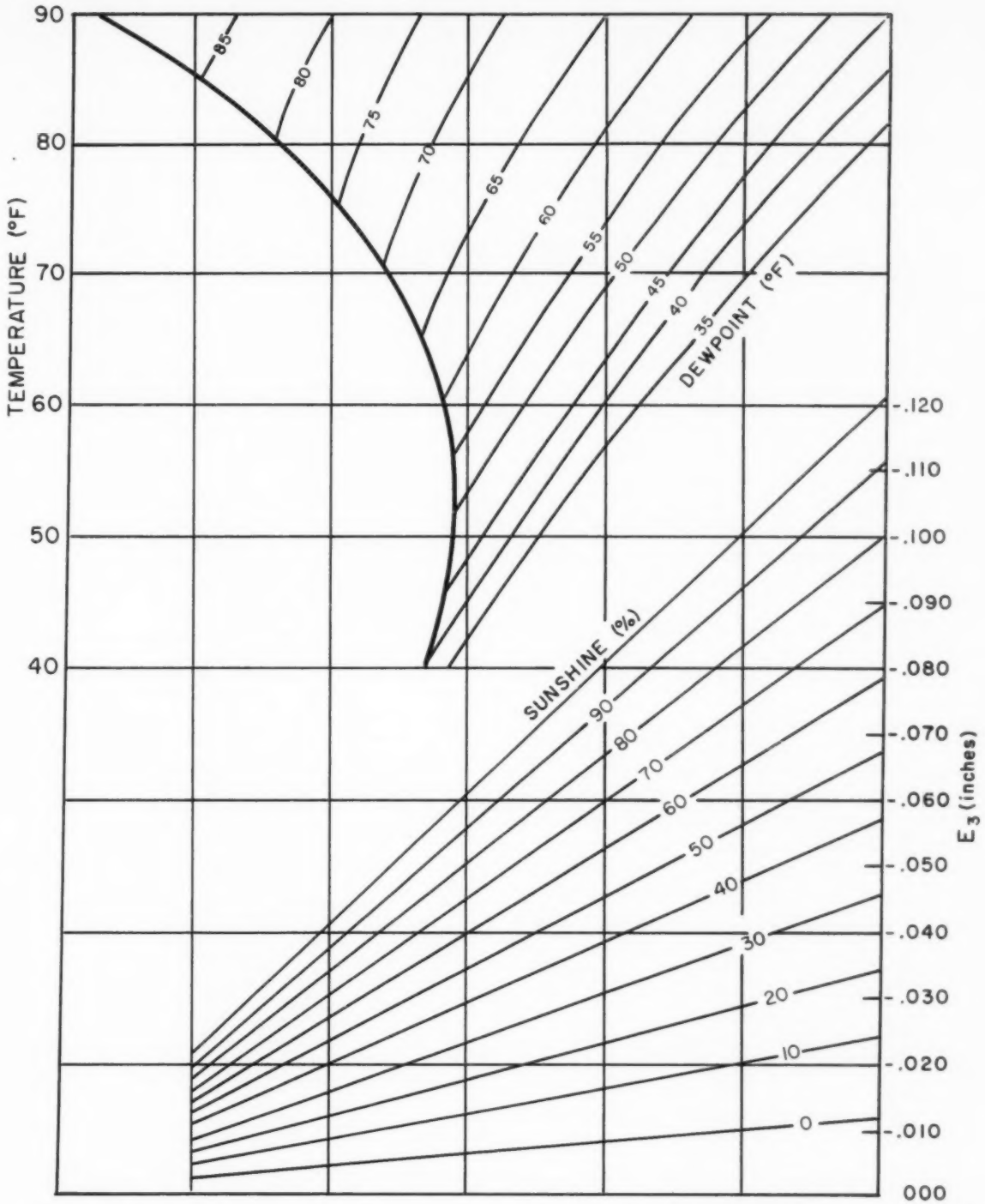

FIGURE 3.—Third of three graphs for computation of potential evapotranspiration by Penman formula. This graph yields E_3 as given by equation (8). To use the graph, (1) enter temperature on the upper left scale, (2) move horizontally to dew point, (3) descend vertically to sunshine percentage, and (4) move horizontally and read value of E_3 on the lower right scale. Note that the values of E_3 are negative. The computed value of potential evapotranspiration, E_t, is given as the algebraic sum of E_1, E_2, and E_3 obtained from figures 1, 2, and 3, respectively.

591682—61——2

A graphical solution of the Penman formula can be devised from the three terms on the right side of (4). Thus

$$E_t = E_1 + E_2 + E_3 \tag{5}$$

where

$$E_1 = \frac{(.7)(.0394)}{D+.27} DR_a(1-r)(.18+.55\, n/N) \tag{6}$$

$$E_2 = (.27)(.35)(e_a - e_d)(.5+.0098\, u_2)\frac{(.7)(.0394)}{D+.27} \tag{7}$$

$$E_3 = -(D)\frac{(.7)(.0394)}{D+.27} ST_a^4(.56-.092\sqrt{e_d})(.10+.90\, n/N). \tag{8}$$

Figure 1 is the graphical solution of equation (6). Since D is a function of the air temperature, the upper part of figure 1 is drawn as temperature versus R_a, the extraterrestrial radiation, while the lower portion of the figure accounts for the influence of the variable n/N. The extraterrestrial radiation for any particular location is fixed by the date of the year. The reader may find complete tables of R_a values for all latitudes in the *Smithsonian Meteorological Tables* [5]. It is possible, therefore, to adapt figure 1 to any fixed location by labeling the indicated isolines of R_a with the corresponding dates for that location. To use figure 1 the reader should enter the upper left hand margin with the air temperature, move to the right until the proper R_a is intersected, then descend to the n/N value. The solution E_1 is then found on the lower right hand margin.

Figure 2 is the graphical solution of equation (7). The upper portion of this figure solves the actual and saturation vapor pressure functions. The relation at the bottom of the figure accounts for the effect of wind speed. To use figure 2, enter the upper left hand margin with the actual air temperature, move horizontally to the dewpoint, then descend to the wind speed curve. The solution E_2 is found on the extreme lower right hand margin.

It should be noted that the wind speed u_2 is that recorded at the 2-m. level. If this value is not known, a measurement at a height h may be converted by use of

$$u_2 = \frac{u_h \log 6.6}{\log h} \text{ or } u_h = \frac{u_2 \log h}{\log 6.6}$$

where the height of measurement is in feet. Thus this figure can be adapted to any particular site by relabeling the wind speeds with the corresponding values for the particular anemometer height; e.g., for 36 ft. as applicable to the Columbia, S.C., anemometer, given by the second set of wind speed labels.

Figure 3 is the graphical solution of equation (8). The upper portion of this figure solves the temperature-vapor pressure relation. The lower part of the graph accounts for the influence of the parameter n/N. To use figure 3, enter the upper left hand margin with the air temperature, move horizontally to the dew point, then descend vertically to the percentage of sunshine. The answer E_3 is found on the lower right hand margin.

The solution E_t to equation (4) is then accomplished by adding results E_1, E_2, and E_3 found from figures 1, 2, and 3. For example, at Columbia, S.C., on May 1, with average temperature 80° F., dew point 70° F., wind speed 8 m.p.h., and sunshine 10 percent, figure 1 gives $E_1 = 0.072$ in.; figure 2 gives $E_2 = 0.025$ in.; and figure 3 gives $E_3 = -0.011$. Thus, from equation (5)

$$E_t = 0.072 + 0.025 - 0.011 = 0.086 \text{ in.}$$

3. CONCLUSION

This paper presents a graphical solution of the Penman formula as adapted for Columbia, S.C. The graphical solution is given in the form of three graphs (figs. 1, 2, 3) which may be adapted for any location by changing figures 1 and 2 as described in the text.

ACKNOWLEDGMENT

The graphs described in this paper were developed during a joint study of the Penman formula by Mr. Nathan Kronberg, Weather Bureau State Climatologist for South Carolina, and the writer. The writer is indebted to Mr. Kronberg for his assistance, review, and encouragement in preparing this graphical presentation.

REFERENCES

1. H. L. Penman, "Natural Evaporation from Open Water, Bare Soil, and Grass," *Proceedings of the Royal Society of London*, Series A, vol. 193, 1948, pp. 120–145.
2. P. J. Rijkoort, "A Nomogram for the Determination of Pan Evaporation Adapted from the Penman Method," *Report 11–143* Royal Netherlands Meteorological Institute, 1954.
3. W. van der Bijl, "Evapotranspiration Problem: First Contribution," Kansas State College, Dept. of Physics, *Report 1956–1957* on Contract Cwb–8806, 94 pp.
4. N. Kronberg and J. C. Purvis, Potential Evapotranspiration Study, unpublished, 1957.
5. R. List (ed.), *Smithsonian Meteorological Tables*, 6th Rev. Edition, Smithsonian Institution, Washington, D.C., 1951.

ON VERIFICATION OF UPPER-AIR WINDS BY VERTICAL SHEAR AND EXTREMES

OSKAR M. ESSENWANGER*

Research Laboratory, Army Ballistic Missile Agency, Huntsville, Ala.

ROBERT E. BRADFORD

National Weather Records Center, U.S. Weather Bureau, Asheville, N.C.

and

WILLIAM W. VAUGHAN**

Marshall Space Flight Center, National Aeronautics and Space Administration, Huntsville, Ala.

[Manuscript received November 23, 1960; revised February 17, 1961]

ABSTRACT

The existence of undetected errors in recorded wind observations may have a biasing influence on a statistical study. In the progress of some studies it has been found necessary to reexamine the data being used. A series of upper-air winds has been checked by using available listings of vertical shear and extreme winds. The developed procedure permits correction for major errors and tolerates the minor (random) errors.

The test of data by maximum wind profiles uses the highest and second highest scalar wind speed for each station and checks the data by profile scan. The test of data by vertical wind shear uses a critical value, theoretically derived, exceedance of which marks the data as suspicious. A detailed check of the wind observation verifies this suspicious value or it is corrected. In this program 3.5 percent of the observations [1] proved suspicious and 85 percent thereof, that is, 2.9 percent of the observations, required correction. Thus the critical value is highly efficient.

The errors were traced and split into clerical errors (1.1 percent), instrumental errors (1.3 percent), and computational errors (0.5 percent), which are quite within reasonable limits.

1. INTRODUCTION

For use in missile design and performance studies by Army Ballistic Missile Agency, basic upper-air wind observations were obtained for locations in the Pacific Ocean, North America, and Europe. The stations are listed in table 1. Preliminary analysis of the data revealed that there were occurrences of apparent errors in the observations as presented on punched cards. It was decided that these data should be checked.

Although it was considered desirable to check and verify all the upper-air data, this was not possible because of the cost and the time required to review the mass of observations. Instead it was decided to establish a checking program which would permit a review eliminating major errors, yet tolerating minor (random) errors. It was considered to be sufficient to restrict the checking process to higher wind magnitudes and wind shears, where the possibility exists that the reported extreme wind velocity arises from the addition of wind data and error with the same sign.

This method permitted the correction of the major items (maximum wind speed and wind shear) required for missile design studies and verification of the wind data at the same time.

The mass of punched cards was converted to magnetic tapes for use on high-speed electronic computers (IBM 704 and 709). Use of these computers permitted the rapid searching of the data and machine listings of all observations (plus the associated profile) which produced the higher wind speeds and wind shear for each altitude level. Also, it was possible to provide preliminary frequency distributions of the wind shear and speed data for use in further evaluation of suspicious data. The corrected observations were subsequently incorporated into the original data records and utilized on various statistical programs for use in missile design and employment studies.

2. THEORETICAL BACKGROUND

The problem existed that frequency distributions for wind shears and extreme values had been programmed, and tabulations similar to table 2 (described later) had been made before the necessity for critical review and correction became apparent. Thus, the problem was not to establish a suitable statistical theory of fitting extreme value data, but rather to develop an economical tech-

*Formerly associated with the National Weather Records Center, U.S. Weather Bureau, Asheville, N.C.

**Formerly associated with the U.S. Army Ballistic Missile Agency, Huntsville, Ala.

[1] "Observation" used here refers to the entire ascent though sometimes only the value at a single level had to be corrected.

TABLE 1.—*Station listing of verified wind data* [1]

Job station No.	Station name	WBAN No.	Period of record	Hour [2] (GMT)	Type of equipment [3]
1	Cocos (Patrick AFB)	12867	1/51- 9/52	00, 12	4, 6, 8
			10/52-11/56	00, 12	8
	Cape Canaveral	12868	11/56-12/57	00, 12	8
2	Tokyo (Haneda AFB)	43311	1/51- 4/52	00, 12	2, 6
			4/52-12/53	00, 12	8
			7/55-12/55	09, 21	8
			8/57-12/57	06, 18	8
	Nagoya	43312	1/54- 6/55	00, 12	8
			1/56- 5/57		8
3	Fairbanks	26411	1/51-12/57	00, 12	6
4	Tripoli (Wheelus AB)	33123	1/51- 4/53	00, 12	2, 6
			5/53-12/57		8
5	Berlin	35140	1/51- 6/55	00, 12	6
6	Wiesbaden	35010	1/51- 3/53	00, 12	6
			4/53- 6/55	00, 12	8
7	Bitburg	34049	1/56-12/57	00, 12	8
8	Port Lyautey	13017	1/51-10/51	00, 12	6
			12/51-12/52		6
			1/53-12/57		8
9	Thule	17605	1/51- 3/54	00, 12	6
			5/55		8
			1/56-12/57		8
10	Libue	22536	1/51-12/57	00, 12	6
11	Grand Bahama Isl	12712	1/51-12/57	00, 12	8
12	International Falls	14918	1/51- 9/54	00, 12	6
			10/54-12/57		8
13	Guam (Anderson AFB)	41414	1/51- 4/53	00, 12	6
			5/53-12/57		8
14	San Juan	11631	1/51- 5/55	00, 12	6
			1/56-12/57		6
15	Balboa, C.Z. (Albrook AFB)	10701	1/51-11/53	00, 12	6
			11/53- 4/55		8
			6/55- 7/55		8
			9/55-12/57		8
16	Johnston Isl. AFB	21601	1/51- 4/53	00, 12	6
			5/53- 2/54		6, 8
			3/54-12/57		8
17	Luzon (Clark AB)	41207	1/51- 8/53	00, 12	6
			9/53-12/57		8
18	Santa Maria	23236	1/51-10/54	00, 12	6
		23273	11/54-12/57		6
19	Keflavik (Meeks Fld)	16204	1/51- 8/51	00, 12	8
		16201	9/51-12/57		8
20	Silver Hill (Washington, D.C.)	93722	1/51-12/52	00, 12	6
			1/53-12/57		8
21	Adak	25704	1/51- 5/53	00, 12	6
			6/53-12/57		8
22	El Paso	23044	1/51- 4/54	00, 12	2
			5/54-12/57		6
23	Barrow	27502	1/51-12/57	00, 12	6
24	Alert	18601	7/53- 6/58	00, 12	6

[1] The sequence of stations is not identical with that in tables 2 or 4.
[2] Prior to May 1957 observations were taken at 03 and 15 instead of 00 and 12. This is not listed here.
[3] Type of equipment: 2=Rabal, single theodolite
4=SCR-584 and SCR-545
6=SCR-658
8=GMD-1 and GMD-1A

nique with minimum amount of time and cost using these available tabulations for selection and checking procedures.

From the statistical point of view it must be pointed out that the problem of establishing profiles of maximum wind speed (magnitude of wind vector) or distributions of maximum wind shears should be approached otherwise than shown in this report by employing an extreme value statistic. However, frequency distributions of maximum wind speed and wind shear in the upper air are not completely known and application of techniques similar to Thom's [2, 3] method or Gumbel's [1] theory would have made necessary the careful evaluation of several such statistical systems. This time-consuming basic study could not have been completed within the limitation of the available time and funds.

The first part of the verification program, checking maximum wind profiles, was relatively simple. The listed and plotted profiles were scanned for suspicious values. Verification of those values considered suspicious was performed by reference to the original data records. Details of the procedures employed are presented in section 3.

The selection of suspicious values for wind shear data appeared very complicated in the beginning. Distributions of wind component shear frequencies were available in the form of table 2 without the column marked "Essenwanger's sum". In the form shown in table 2, frequency distributions were given without regard to algebraic sign of the wind shear. The problem was to find a value which separated the acceptable values from suspicious values without reviewing too many observations or accepting a large amount of unreliable data. This value will be called the critical value ϵ_c.

The column marked "99.865" was practically identical with the maximum shear value. There is no reason to expect all maximum shear values to be wrong. On the other hand, the value listed in the column marked "97.72" was assumed to be acceptable since regularly it was exceeded by 2 out of every 100 values. Thus we may contemplate the following ideas.

We start with the assumption that zonal and meridional wind components are normal (Gaussian) distributions, or approximately normal. Departures from normality will be introduced later in the discussion. The wind shear data must then also follow a normal distribution. The shear distribution, disregarding the sign, then is a folded distribution. This folding occurs at the zero wind shear value. The mean value of the frequency distribution of zonal or meridional shear values, not disregarding the sign, usually will not coincide with zero. The question is now: Which portion of σ (standard deviation) corresponds to the listed percentage frequencies, 50, 84.1, 97.72, etc.?

If the folding occurs outside the $\pm 3\ \sigma$ value [2] in reference to the mean, then practically all shear values have the same sign. Then the shear distribution follows a normal distribution and the 50 percent value (median) virtually coincides with the mean. This statement holds for folding above $\pm 1.5\ \sigma$ (fig. 1a) if we assume that the frequency of data above $3\ \sigma$ is negligible. If the folding is within $\pm 1.5\ \sigma$, then the mean value of the unfolded normal distribution must be smaller than the 50 percent value (fig. 1b). Thus the listed 50 percent value permits evaluation of the magnitude of this mean value. We recognize (see also table 2) that for practical purposes this value is so close to the zero wind shear that we can continue our discussion about the folded distribution as if it were folded at the mean value zero. Then the 84.1 percent value corresponds to $1.41\ \sigma$, the 97.72 percent to $2.28\ \sigma$, and the 99.865 percent to $3.20\ \sigma$.

We build the ratio

$$\frac{99.865 \text{ percentage value}}{97.72 \text{ percentage value}} = \frac{3.20\sigma}{2.28\sigma} = 1.40$$

Thus, theoretically we should expect the factor 1.4. A

[2] Some statisticians may want to use the symbol s, the estimate of the population standard deviation σ. This has no influence upon the development in this paragraph insofar as later the 84.1 or 97.72 value may express the empirical replacement for σ or s.

TABLE 2.—*Meridional wind shear (sec.$^{-1}$) distributions at Keflavik, Iceland, for January. Station altitude, 54 m. MSL; latitude, 63°57′ N.; longitude, 22°37′ W.; period of observations, January 1951–December 1957*

Altitude km. (MSL)	Number of OBS	Cumulative Percentage Frequency							Essen-wanger's sum	Max shear	Pct. freq.	Suspicious values
		.135	2.28	15.9	50.0	68.0	84.1	97.72	99.865				
SFC-0.5	372			.0026	.0060	.0131	.0202	.0369	.0808	.0621	.0808	.27	*
0.5-1.0	370			.0008	.0037	.0055	.0093	.0199	.0291	.0342	.0291	.27	
1.0-1.5	368				.0030	.0055	.0092	.0227	.0314	.0369	.0314	.27	
1.5-2.0	369			.0001	.0028	.0046	.0090	.0176	.0343	.0316	.0343	.27	*
2.0-2.5	372				.0028	.0042	.0077	.0153	.0306	.0280	.0306	.27	*
2.5-3.0	374				.0037	.0057	.0085	.0204	.0319	.0339	.0319	.27	
3.0-4.0	375			.0004	.0027	.0040	.0061	.0103	.0163	.0214	.0163	.27	
4.0-5.0	373			.0003	.0021	.0038	.0064	.0139	.0267	.0253	.0267	.27	*
5.0-6.0	371			.0004	.0027	.0049	.0080	.0164	.0724	.0294	.0724	.27	*
6.0-7.0	359				.0023	.0042	.0069	.0166	.0656	.0285	.0656	.28	*
7.0-8.0	351			.0002	.0025	.0042	.0074	.0157	.0333	.0281	.0333	.28	*
8.0-9.0	335				.0028	.0043	.0074	.0159	.0480	.0283	.0480	.30	*
9.0-10.0	303				.0023	.0038	.0074	.0172	.0345	.0296	.0345	.33	*
10.0-11.0	278			.0004	.0028	.0049	.0088	.0243	.0390	.0381	.0390	.36	*
11.0-12.0	262			.0003	.0028	.0047	.0085	.0199	.0383	.0334	.0383	.36	*
12.0-13.0	249				.0027	.0042	.0085	.0176	.0277	.0311	.0277	.40	
13.0-14.0	231				.0027	.0054	.0085	.0140	.0256	.0275	.0256	.43	
14.0-15.0	207				.0020	.0042	.0073	.0142	.0242	.0265	.0242	.48	
15.0-16.0	187				.0018	.0040	.0071	.0126	.0194	.0247	.0194	.53	
16.0-17.0	170				.0019	.0042	.0077	.0162	.0192	.0289	.0192	.59	
17.0-18.0	156				.0021	.0049	.0092	.0172	.0234	.0314	.0234	.64	
18.0-19.0	138				.0026	.0045	.0069	.0142	.0150	.0261	.0150	.72	
19.0-20.0	115				.0017	.0035	.0071	.0150	.0219	.0271	.0219	.87	
20.0-21.0	100				.0015	.0046	.0099	.0157	.0198	.0306	.0198	1.00	
21.0-22.0	89				.0021	.0042	.0085	.0176	.0289	.0311	.0289	1.12	
22.0-23.0	75				.0014	.0035	.0064	.0163	.0269	.0277	.0269	1.33	
23.0-24.0	65				.0017	.0042	.0074	.0214	.0290	.0338	.0290	1.54	
24.0-25.0	46				.0019	.0033	.0058	.0222	.0255	.0330	.0255	2.17	
25.0-26.0	36				.0014	.0042	.0092	.0211	.0211	.0353	.0211	2.78	
26.0-27.0	19				.0011						.0127	5.26	
27.0-28.0	12				.0011						.0127	8.33	
28.0-29.0	8										.0240	12.50	*
29.0-30.0	6										.0031	16.67	*
30.0-31.0	2										.0008	50.00	*
31.0-32.0	2										.0046	50.00	*
32.0-33.0	2										.0027	50.00	*
33.0-34.0	2										.0073	50.00	*
34.0-35.0	2										.0008	50.00	*
35.0-36.0	2										.0157	50.00	*
36.0-37.0	2										.0074	50.0	*
37.0-38.0	1										.0008	100.0	*
38.0-39.0	1										.0153	100.0	*
39.0-40.0													
40.0-41.0													

review of the frequency tabulations showed that for the meridional shear the average empirical value amounts to 1.8 and for the zonal shear it is between 1.5 and 1.7. The factor 1.6 seems, therefore, a sound compromise between theory and practice. This takes care of departures from the normal distribution law and a mean value different from zero.

We have now established a theoretically acceptable critical value (ϵ_c) of 1.6 times 2.28 σ, which equals 3.65 σ. If the σ is known, we can easily compute this critical value ϵ_c.

We also could use the 97.72 percentage value for the 2.28 σ value. For the individual case, however, too many random variations may influence the result. Therefore, we may try to incorporate another procedure to decrease this effect. When we add the 84.1 percent and the 97.72 percent values, we obtain 1.41σ plus 2.28σ, which equals 3.69σ. This is very close to 3.65σ. Thus we may derive the critical value by employing the 84.1 and 97.72 percentage values.

Further consideration may be given to an observation tolerance error. An error of 5 m. sec.$^{-1}$ per 1000 m. for those extreme values seems to be within the limitation of measurements.[3] Thus we tolerate this error for the critical value and derive finally

$$\epsilon_c = P_{84.1} + P_{97.72} + 0.005 \text{ sec.}^{-1}$$

where $P_{84.1}$ is the 84.1 percentage value and $P_{97.72}$ the 97.72 percentage value.

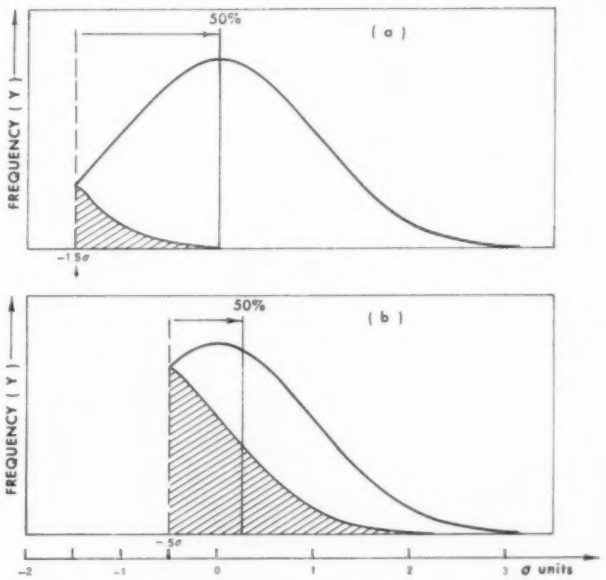

FIGURE 1.—Folding of normal distribution and relation to 50 percent line (median).

[3] The first 3000 m. in table 2 are listed in 500-m. layers. It was decided for simplicity to adopt 0.005 sec.$^{-1}$ for those 500-m. layers, too.

The unit of ϵ_c is the same as in table 2, namely inverse seconds. From table 2 we may give a sample for computation of the critical value for the layer, surface to 0.5 km. It would be

$$\epsilon_c = .0202 + .0369 + .0050 = .0621 \text{ sec.}^{-1}$$

This value is listed in table 2 in the column titled "Essenwanger's sum". All shear observations exceeding this value as computed for each level were labeled suspicious. They are marked by an asterisk in table 2. Further description of the shear checking process will follow in section 4. Of the suspicious values, 85 percent had to be corrected, which is considered as high efficiency for this checking procedure.

Results of randomly picked shear values for checking have demonstrated that efficiency drops sharply for values below the critical value. Thus, by the outlined process we have achieved the goal to eliminate major errors, and tolerate (random) minor errors which have little bearing upon the determination of missile design criteria.

3. TEST OF DATA BY MAXIMUM WIND PROFILES

The highest and second highest (scalar) wind speeds for each of the stations at each of the 45 levels (or to the highest level attained if it was less than 41 km.) were machine selected, and the observations [4] containing these high wind speed values were listed.

The verification of these speeds may be managed in two ways: verify or correct each and every value, or locate and correct the greater majority of the erroneous values, particularly values that are very large or appear to be inconsistent with a smooth profile which would be expected if all observations were correct. Practical economic considerations demanded that the latter be the guiding principle in the verification. One-third, or 8, of the stations received total verification; i.e., every high wind speed value was checked to provide a basis of comparison to determine the adequacy of the smooth profile verification procedure.

The verification procedure was divided into three steps or categories, namely: observation scan, terminating values, and profile scan. The sequence of the checking process might have been arbitrarily established, however, it appeared that the sequence listed above would provide maximum assurance that the final product, the maximum wind profile, was correct.

[4] The word "observation" in this report is used in the sense of characterizing the entire ascent as one taken observation and is in this way different from an observed value.

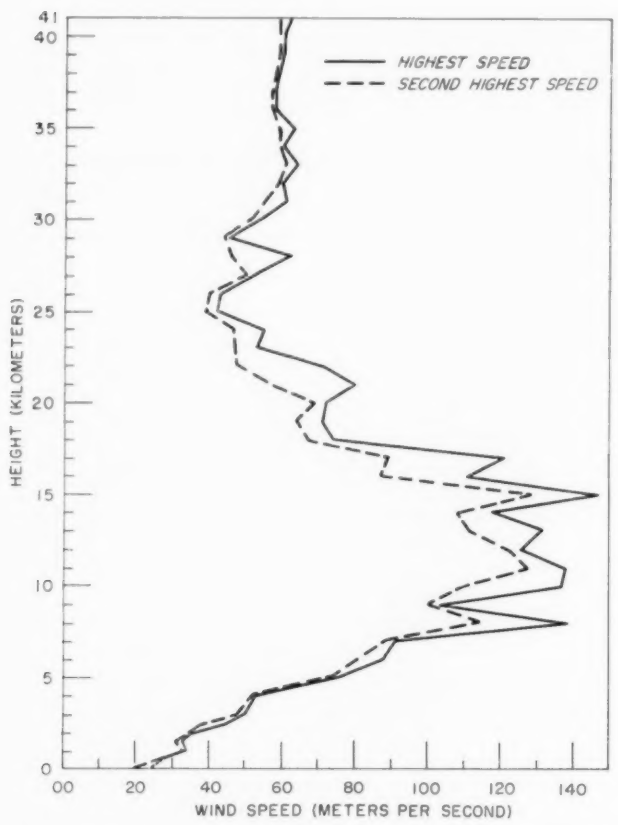

FIGURE 2.—Maximum wind profile before verification, station no. 1.

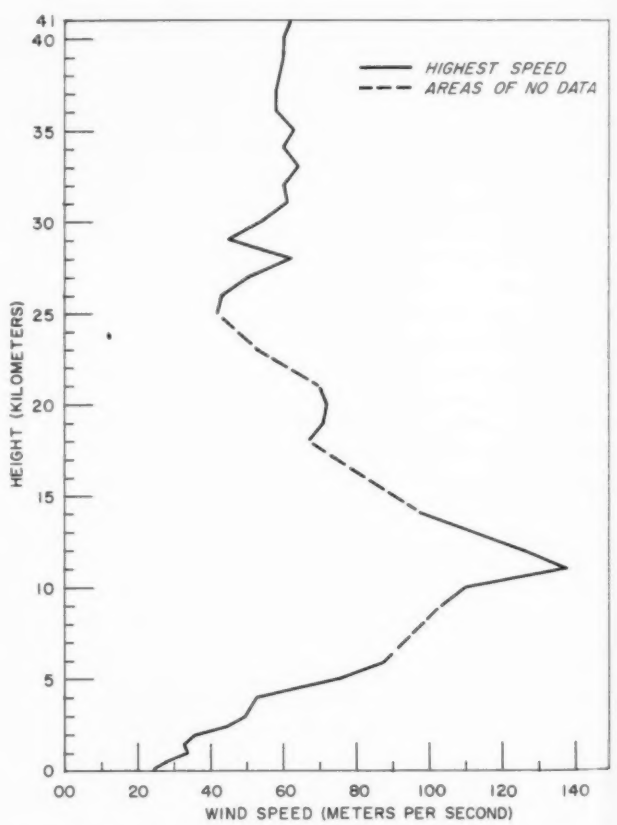

FIGURE 3.—Maximum wind profile after verification, station no. 1.

The observation scan was literally a visual scan of the observation. Each machine-selected observation was searched for apparent inconsistencies, such as a speed of 10 m.p.s. followed at the next level by a speed of 116 m.p.s., or similar rapid and large fluctuations in wind speed. Those observations containing such inconsistencies were checked and corrected as appropriate. This subjective scanning sufficed for errors detectable by discontinuity. Were all errors of this type, no further checking had been necessary. But though some profiles showed considerable smoothing from this process, most profiles still contained irregular contours which appeared suspicious. The checking process was therefore continued.

Each value occurring as the terminating speed for a given observation was considered suspicious. All observed wind values are the result of 2- or 4-minute averages except the last speed obtained which is allowed to be a 1-minute calculation if a 2- or 4-minute average is not available. Terminating values were therefore checked for representativeness. This eliminated the error from terminating fluctuations, but further smoothing was needed.

The profile scan necessitated the construction of the vertical profiles of these highest and second highest wind speeds. Figure 2 pictures the original profiles for station no. 1 to serve as an example. The first move was to apply to the profiles all corrections resulting from the first two steps of the verification procedure. The profiles, after this preliminary correction, were then examined and questionable values were "picked off" for verification. It is obvious that a great deal of subjectivity was also encountered here, but a system was utilized. The values were chosen in sets, each set being verified and the resulting corrections applied before the next set was chosen. Each set consisted of those wind speed values which, if changed, would most smooth the contours of the profile. This set checking process was continued until no errors were found or so few were found that the profile was virtually unaffected.

Figure 3 shows the maximum wind profile after verification. Since this investigation dealt with only the highest and next to highest speeds, and values to replace these when they were deleted or changed to a value below that of the second highest were not included in this profile, thus dashed areas of no data appear. This meant the highest or second highest wind speed for a dashed level would have to be obtained by going back to the original records and selecting the now highest (or second highest) value. As this would have had to be done by hand at National Weather Records Center, it was decided to leave the profile as in figure 3. The missing values may easily be replaced by machine selection at Army Ballistic Missile Agency. The corrected profile, in

TABLE 3.—*Maximum wind verification (observations checked and changed)*

Station*	1	2	3	4	5	6	7	8	9	10	11	12
	Number of observations	Observations checked	Observations changed	Percent of observations checked Column 2 / Column 1	Percent of observations changed Column 3 / Column 1	Percent of observations checked, changed Column 3 / Column 2	Number of profile points	Points checked	Points changed	Percent of points checked Column 8 / Column 7	Percent of points changed Column 9 / Column 7	Percent of points checked, changed Column 9 / Column 8
By procedure:												
1	62	31	23	50	37	74	90	40	23	44	26	58
2	68	38	27	56	40	71	90	48	29	53	32	60
3	69	30	3	43	4	10	64	40	3	63	5	8
4	58	25	18	43	31	72	90	55	23	61	26	42
5	75	24	9	32	12	38	72	40	17	56	24	43
6	48	27	19	56	40	70	90	69	38	77	41	55
7	51	21	0	41	18	43	90	53	11	59	12	21
8	56	40	23	71	41	58	90	69	37	77	41	54
9	48	27	6	56	13	22	86	56	6	65	7	11
10	86	38	8	44	9	21	64	37	8	58	13	22
11	64	36	18	56	28	50	90	61	24	68	27	39
12	50	21	9	42	18	43	65	36	10	55	15	28
13	90	32	19	53	32	59	90	58	32	64	36	55
14	86	35	20	41	23	57	75	39	22	52	30	56
15	73	45	31	62	42	69	90	63	40	70	45	63
16	72	42	33	58	46	79	90	67	49	74	54	73
Totals	1,026	512	275	50	27	54	1,326	831	372	63	28	45
By total verification:												
17	44	44	23	100	52	52	90	90	36	100	40	40
18	64	64	37	100	58	58	70	70	35	100	50	50
19	60	60	45	100	75	75	90	90	60	100	67	67
20	73	73	46	100	63	63	76	76	40	100	53	53
21	55	55	42	100	76	76	86	86	59	100	69	69
22	58	58	28	100	48	48	73	73	39	100	53	53
23	50	50	30	100	60	60	73	73	43	100	59	59
24	59	59	32	100	54	54	72	72	26	100	36	36
Totals	463	463	283	100	61	61	630	630	338	100	54	54
Grand Totals	1,489	975	558	65	37	57	1,956	1,461	710	73	36	49

*The sequence of stations is not identical with station listing in table 1.

general, takes on a smoother appearance with one distinct layer of maximum wind speed. This is true with all of the stations.

Table 3 denotes the amount of checking and changing done in the maximum wind profile verification program. The data are subdivided into two groups; the first being for the 16 stations for which the verification was accomplished by the procedure described in the preceding paragraphs, the second for the 8 stations which received total verification. The combination of these yields the overall results. Table 3 is self explanatory.

As can be seen from table 3, there is some question concerning the efficiency of this three-step procedure, particularly when the percentage of values changed becomes very large. It would seem that there still are a significant number of erroneous observations unchecked. It must be remembered, however, that the criterion for terminating verification was that the contours of the profile remain virtually unchanged, since the original goal of the verification was to obtain a representative maximum wind profile. This goal was attained in all cases where the profile was not completedly destroyed. Three stations lacked sufficient data and for one the entire profile would have needed reconstruction.

This method was designed for adequacy, with efficiency being second in importance. Methods aspiring toward high efficiency may be similar to the above procedures but would necessarily include more objectivity and less subjectivity. The method outlined for vertical wind shear verification with objective selection may be adaptable to wind speeds using similar frequency distributions.

4. TEST OF DATA BY WIND SHEAR

Selections were made from the shear distribution tables similar to table 2. These tables list the vertical shear by 1-km. layers, beginning at 3 km. Below 3 km., 500-m. layers were taken. The first attempt at selection was by picking out values that seemed to be erratic. This was abandoned almost immediately since it was too laborious and uncertain (nearly 14,000 observations contained all of the maximum shear values).

Then it was decided to use the method outlined in section 2. This method is as follows. Obtain the sum of the shear values at the cumulative percentage frequencies of 84.1 percent and 97.72 percent plus 0.0050 $sec.^{-1}$, then select shears for checking on the basis that any shear value greater than this sum is suspicious. In addition, a selection by observations was made: any value that had been obtained at a level reached ten or less times during the period of record was considered as suspicious, regardless of magnitude.

The selection of the suspicious values is demonstrated in table 2. This tabular form portrays layer versus cumulative percentage frequency with supplementary columns for observations counts and the observed maximum shear. The vertical wind shear (henceforth shear) values were computed for both the zonal and meridional components. Listings of the profile for the maximum wind shear accompanied the listings of the form of table 2.

In the first set of tabulations maximum shear values only were subjected to verification. Later all shear values exceeding the "critical" threshold (Essenwanger's sum) were listed as a review program. It was understood that, regardless of what portion or portions of an observation first raised suspicion, the entire observation was to be subjected to a checking process.

Secondary review was limited to a review check program which was designed to encompass not only highly suspicious observations not contained in the first phase, but also observations in which errors may have occurred or been overlooked during previous verification. The latter, fortunately, occurred very few times. Even with this, some few errors undoubtedly still escaped detection.

The combination of these methods has proven acceptably efficient in that 85 percent of the observations selected as suspicious were found to be erroneous.

The errors have been tabulated in three categories: clerical, instrumental, and computational. The clerical errors were based on the premise that no technical observer training was required to perform the work classified as clerical. They were subdivided into three types: punching, extraction (or transcription), and plotting of Form WBAN 20A. The punching was, of course, the production of the cards constituting the original card decks. The extraction was the "picking off" of values from the WBAN 20A, a plot of the observed data in the form of wind speed and direction versus height. Plotting refers to wrong plots of WBAN 20A.

Instrumental error may be defined as large and rapid fluctuations in angles (azimuth and elevation) incompatible with the calculated height changes.

The computational error was subdivided into two types: Calculations on WBAN 20 (the observer's work sheet) and fictitious ascension rates (of the balloon) as calculated from erroneous pressure-temperature-time measurements. Fictitious ascension rates may be thought of as instrumental, but only the tracking equipment was considered an instrument in this study. The tracking equipment consisted mainly of the theodolite (visual tracking), the SCR–658 (manual radiosonde tracking), and the GMD–1 and GMD–1A (automatic radiosonde tracking).

Table 4 shows the error statistics resulting from the verification of the shear selected observations. The headings are self explanatory. Some observations contained more than one type of error so that the occurrence of errors exceeds the number of observations changed. The end results in this tabulation prove interesting in the predominance of the instrumental and clerical errors. The relatively small computational error is gratifying.

We note in table 4 that from all observations only 3.5 percent were found to contain suspicious values; from the suspicious observations 85 percent, i.e., 2.9 percent of all

TABLE 4.—*Vertical wind shear verification (error statistics)*

Station*	Observations				Number of errors				Percentage of				Percentage of total errors		
	1	2	3	4	5	6	7	8	Total observations containing maximum shear Column 2 / Column 1	Total observations containing suspicious Column 3 / Column 1	Suspicious changed Column 4 / Column 3	Changed of total Column 4 / Column 1	Clerical Column 6 / Column 5	Instrumental Column 7 / Column 5	Computation Column 8 / Column 5
	Total number	Containing maximum shear	Suspicious	Changed	Total	Clerical	Instrumental	Computation							
1	5,114	595	226	159	167	92	57	18	11.6	4.4	70	3.1	55	34	11
2	4,992	556	223	194	249	101	93	55	11.1	4.5	87	3.9	41	37	22
3	5,114	537	169	133	134	27	100	7	10.5	3.3	80	2.6	20	75	5
4	5,114	626	208	159	166	78	58	30	12.2	4.1	76	3.1	47	35	18
5	3,652	550	106	87	107	33	50	24	15.1	2.9	82	2.4	31	47	22
6	5,114	602	215	195	219	106	73	40	11.8	4.2	91	3.8	48	34	18
7	1,462	515	112	83	97	38	15	44	35.2	7.7	74	5.7	39	16	45
8	5,054	542	146	118	152	47	53	52	10.7	2.9	81	2.3	31	35	34
9	3,896	504	124	91	102	72	26	4	12.9	3.2	73	2.3	71	25	4
10	5,114	608	163	80	75	37	35	3	11.9	2.0	78	1.6	49	47	4
11	5,114	627	178	162	189	60	66	63	12.3	3.5	91	3.2	32	35	33
12	5,114	535	182	121	152	77	58	17	10.5	3.6	66	2.4	51	38	11
13	5,114	612	182	167	212	84	69	59	12.0	3.6	92	3.3	40	32	28
14	4,686	619	112	90	121	39	48	34	13.2	2.4	80	1.9	32	40	28
15	4,980	622	150	132	167	73	60	34	12.5	3.0	88	2.6	44	36	20
16	5,114	640	226	219	287	132	86	69	12.5	4.4	97	4.3	46	30	24
17	5,114	650	223	195	267	105	104	58	12.7	4.4	87	3.8	39	39	22
18	5,114	591	129	117	127	24	91	12	11.6	2.5	91	2.3	19	72	9
19	5,114	541	251	237	300	129	120	51	10.6	4.9	94	4.6	43	40	17
20	5,114	549	127	116	121	9	104	8	10.7	2.5	91	2.3	7	86	7
21	5,114	486	217	198	227	47	139	41	9.5	4.2	91	3.9	21	61	18
22	5,114	509	77	61	64	12	46	6	10.0	1.5	79	1.2	19	72	9
23	5,114	521	162	146	164	39	113	12	10.2	3.2	90	2.8	24	69	7
24	3,652	502	103	80	93	35	49	9	13.7	2.8	78	2.2	38	52	10
Grand total	114,208	15,639	3,951	3,340	3,959	1,496	1,713	750	11.9	3.5	85	2.9	38	43	19

*The sequence of stations is not identical with station listing in table 1.

observations, had to be changed. This means that one or several values had to be corrected in 2.9 percent of the observations. As one observation contains numerous levels, the actual percentage of errors in relation to the wind data of all levels is far less. The clerical error contributed 1.1 percent, the instrumental error 1.3 percent, and the computational error 0.5 percent. A perfect card deck would be the ideal goal, of course. As one should expect, this goal cannot be reached without a thorough check of the produced data. Thus, the magnitude of percentage of the larger error discovered by the method outlined above stays well within reasonable tolerance limits.

A few brief remarks may be in order concerning the difficulties involved in verification. First, the major division of errors is not as clear-cut as it appears. Prior to 1956, the extracted values were not always entered in the allotted space on WBAN 20A. Errors occurring subsequent to plotting were attributed to extraction in such cases. Then, beginning on January 1, 1956, WBAN 20A was no longer a filed form so that plotting errors were undetectable. WBAN 20B had come into being, on which was allotted space for the "extracted" values. Again, arbitrarily, errors occurring between calculation (WBAN 20) and punching were attributed to extraction, so that an overlap occurred. Fortunately, plotting errors contributed very little to the mass of clerical errors.

Perhaps the most difficult problems arose with erratic instrument data and fictitious ascension rates. Balloon heights are determined through pressure-temperature considerations on Forms WBAN 31 A and B. Erroneously low pressure or high temperature readings result in erroneously high height determinations, which when considered with ascension time, may present unduly large ascension rates. This normally occurred in the topmost layers of the higher ascents. This same reasoning can also account for highly erratic or incompatible height changes at any level with the erroneous pressure or temperatures being high or low. Highly erratic angles are caused mainly by equipment malfunction and limitation. Any appreciable influence of turbulence would be confined to the lowest levels except under rare conditions such as balloon entry into a thunderstorm or possibly clear air turbulence. The first event was eliminated by consideration of the weather reports. The latter event, generally not too frequent in occurrence, is not known at the present in sufficient detail to make an unequivocal decision. It was felt, however, that when low ascension rates are involved, it is more likely that the data are erroneous due to instrumental errors. This conclusion may be due for revision after knowledge of clear air turbulence has improved.

In general, erratic data were determined subjectively since there were no adequate objective methods available. Ascension rates were, in general, declared fictitious in a subjective manner since time limitations and unavailable observation data precluded thorough checking. There are two compensating factors, however, in that observation data were always given the benefit of the doubt, and all decisions were made by qualified meteorologists.

5. CONCLUSION

This study has discussed the possibility of checking wind data by maximum wind profiles and wind shear distributions. While the maximum wind profiles were evaluated for suspicious values by profile scan, the checking process by wind shears was based upon computation of a critical value ϵ_c. Exceedance of this critical value made the shear value suspicious and subject to verification.

The derivation of the critical value ϵ_c was developed and the application to 24 stations showed an efficiency of 85 percent, which may be considered very high. Although 3.5 percent of the observations proved to be suspicious, and 2.9 percent had to be corrected, the actual corrections are less, as one observation in the average contains between 20 and 30 level values, not all of which had to be corrected.

The errors were traced and divided into 1.1 percent clerical errors, 1.3 percent instrumental errors, and 0.5 percent computational errors. These are within reasonable limitation.

It may be stressed that establishment of maximum wind profiles or maximum wind shears may be better approached by theoretical statistical processes in order to eliminate the effect of the relatively short period of available data record. Time and cost limitations, however, prevented further investigation in this direction.

ACKNOWLEDGMENTS

The authors wish to express their special appreciation to Mr. Earl M. Ritchie of NWRC, who started work on the maximum wind speed procedure and completed most of this phase of the project. We would like also to recognize the outstanding efforts of Mr. Norman Graham of NWRC for the technical work in the accomplishment of the project.

REFERENCES

1. E. J. Gumbel and P. G. Carlson, "Extreme Values in Aeronautics," *Journal of the Aeronautical Sciences*, vol. 21, No. 6, June 1954, pp. 389–398.
2. H. C. S. Thom, "Frequency of Maximum Wind Speeds," *Proceedings of the American Society of Civil Engineers*, Sgs. No. 539, 1954, pp. 1–11.
3. H. C. S. Thom, "Distribution of Extreme Winds in the United States," *Journal of the Structural Division, Proceedings of the American Society of Civil Engineers*, vol. 86, No. ST 4, Apr. 1960, pp. 11–24.

THE WEATHER AND CIRCULATION OF MARCH 1961[1]

Another Mild Month in the United States

JAMES F. ANDREWS

Extended Forecast Section, U.S. Weather Bureau, Washington, D.C.

1. HIGHLIGHTS

The mild weather of the second half of February 1961 [1] persisted into March as temperatures averaged above seasonal normals in nearly the entire United States (fig. 1). A notable exception was Alaska, where near record cold prevailed. Frequent storminess in the central Plains, associated with a mean trough (fig. 2), brought heavy precipitation and flooding to much of that area. This March was in sharp contrast to March of 1960 [2], a very cold, snowy period in the eastern two-thirds of the Nation.

2. AVERAGE CIRCULATION

The monthly mean circulation patterns at 700 mb. (fig. 2) and sea level (fig. 3) for March 1961 were featured by strong blocking in the Atlantic. This was associated with a band of positive anomaly of both 700-mb. height and sea level pressure around 55° N., and a much deeper than normal trough near mid-Atlantic. In addition, the Icelandic Low was split and displaced southward, a feature commonly associated with blocking.

Blocking was also present over North America, where 700-mb. heights averaged as much as 160 feet above normal over James Bay (fig. 2). A deeper than normal trough extended from mid-United States southwestward. The rather short wave spacing that existed at middle and low latitudes across North America and the Atlantic was quite characteristic of blocking.

Blocking also appeared in the Pacific, where it was related to the center of positive height anomaly near Kamchatka, the deep trough in the Gulf of Alaska at 700 mb. (fig. 2), and the southward displacement of the split Aleutian Low at sea level (fig. 3).

The circulation in polar regions was dominated by a strong High centered north of Alaska at sea level and aloft (figs. 2 and 3). This cell developed strongly near mid-month, concomitant with appearance of a deep cyclonic center in northern Scandinavia. Both cells remained quasi-stationary, reaching their greatest strength during the 5-day period March 23–27 when the maximum mean sea level pressure in the High was 1047 mb. and the minimum in the Low 982 mb.

Over Eurasia the mean circulation was well defined, consisting of a deep trough in eastern Europe flanked by strong ridges, and there was little displacement of these features from sea level (fig. 3) to 700 mb. (fig. 2). The European ridge-trough system was associated with the strongest height anomalies in the Northern Hemisphere (+390 ft. and −470 ft. in fig. 2).

The monthly mean isotach chart and its departure from normal (fig. 4) further reflect the blocking character of the circulation at 700 mb. The jet axis at this level was well defined and displaced south of its normal position over nearly the entire western portion of the Northern Hemisphere. Note also the unusual double jet across the Atlantic. These two jet axes merged in the northeastern Atlantic to produce an extensive area of above normal wind speeds, as much as 11 m.p.s. above normal over southern Scandinavia (fig. 4B).

Wind speeds well above normal were also observed in the eastern Pacific (fig. 4B). As this strong current approached the west coast of the United States, it underwent marked diffluence, aided in part by blocking in Canada.

3. CIRCULATION TRANSITION WITHIN THE MONTH

The most important change in circulation during the month was associated with retrogression of a pronounced blocking wave which developed from a strong ridge over

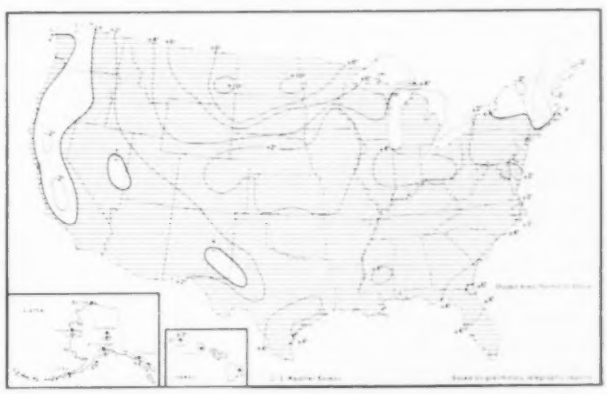

FIGURE 1.—Departure of average temperature from normal (° F.) for March 1961 (from [5]). Mild weather dominated the Nation.

[1] Descriptions of the weather of April, May, and June 1961 will appear in the July, August, and September issues of the *Monthly Weather Review*, respectively.

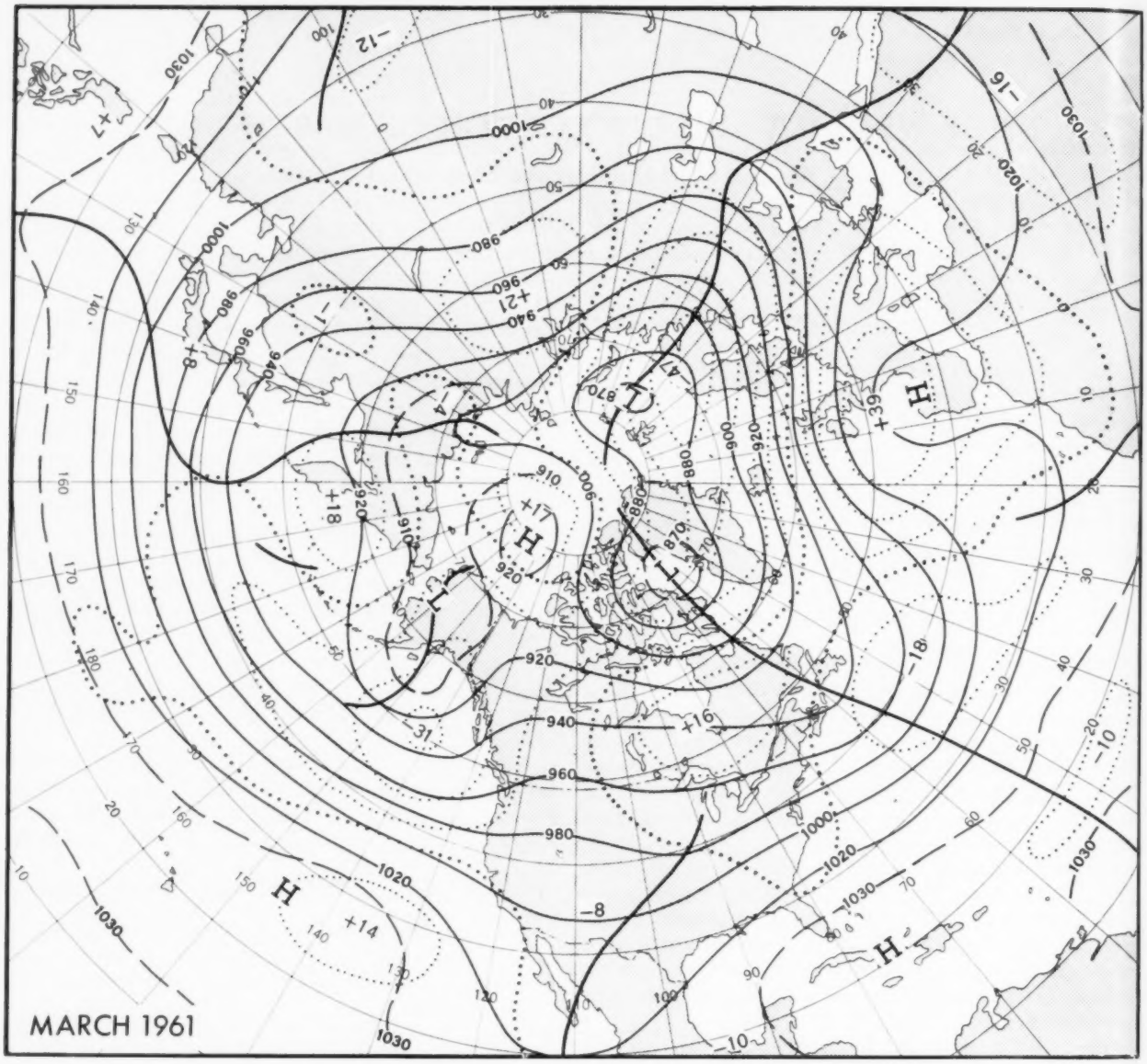

FIGURE 2.—Mean 700-mb. contours (solid) and departures from normal (dotted), both in tens of feet, for March 1961. Blocking at middle latitudes was prominent over North America and the Atlantic.

Europe in February [1]. During March the blocking spread across the Atlantic into North America, accompanied by an abrupt transition from high to low zonal index conditions (fig. 5). The magnitude of this transition in circulation is shown in figure 6, which gives the change in 700-mb. height between the first and last halves of the month. Note the pronounced increase in heights at higher latitudes and falls at lower latitudes over the Atlantic and North America. The greatest change occurred in the Atlantic where 700-mb. heights rose as much as 740 feet.

A further manifestation of this reversal in circulation is obtained by comparing typical 5-day mean patterns of 700-mb. height and sea level pressure observed at time of high index (fig. 7) and low index (fig. 8). Of additional interest are the tracks of primary, migratory cyclones (dashed) and anticyclones (dotted) appearing during these 5-day periods and superimposed on the sea level charts. The high-index patterns (fig. 7) display most of the characteristic features of this type of circulation [3]; i.e., fast zonal westerlies, small wave amplitude aloft, and pressure systems oriented east-west.

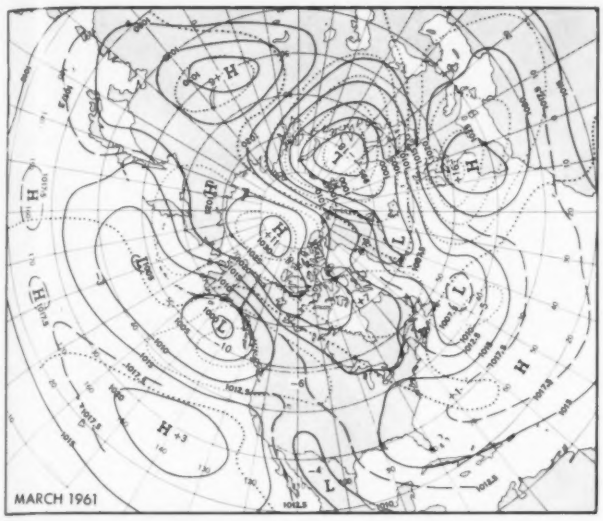

FIGURE 3.—Mean sea level isobars (solid, with intermediate isobars dashed) and departures from normal (dotted), both in millibars, for March 1961. Unusually strong pressure gradients prevailed across Europe and Alaska.

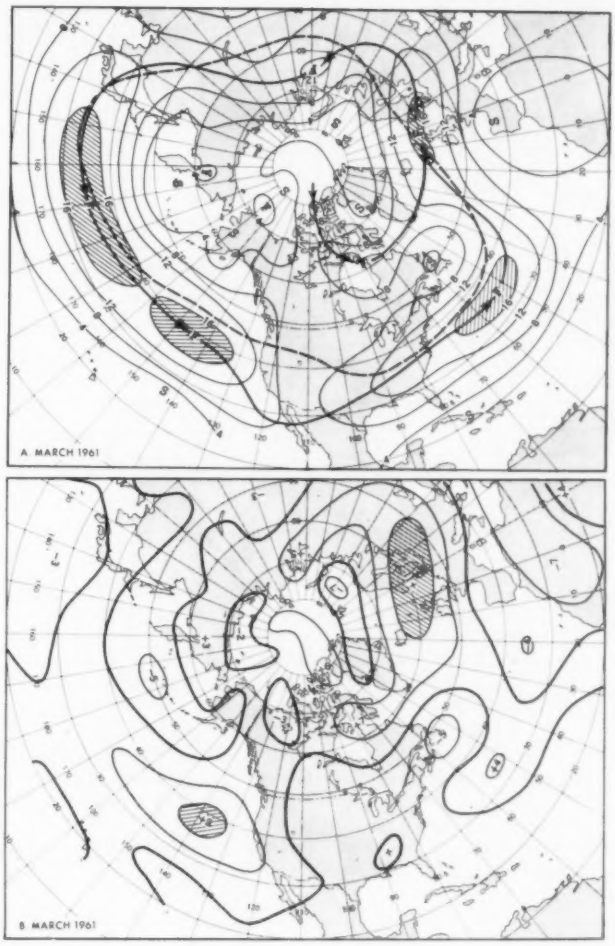

FIGURE 4.—(A) Mean 700-mb. isotachs and (B) departures from monthly normal wind speeds, both in meters per second, for March 1961. Solid arrows in (A) indicate principal axes of maximum wind speeds, and dashed arrows their normal March positions. Regions with wind speeds greater than 16 m.p.s. and anomalies greater than 8 m.p.s. are hatched. The westerlies were south of their normal position over much of the hemisphere.

During the period of lowest index the circulation was characterized by a disruption of the westerlies into closed cellular centers, shorter wavelengths aloft, and a general north-south orientation of pressure systems (fig. 8). In addition, the split storm track in the Atlantic during low index contrasts with the single primary track across the Atlantic during high index. Note also (fig. 8B) the high frequency of slow-moving storm centers in the central United States with low-index conditions. Strong blocking in the Atlantic was evidenced by development of an upper-level "omega" pattern (fig. 8A). Retrogression of blocking into North America was accompanied by development of a similar "omega" pattern in the United States, although not as pronounced as in the Atlantic.

An additional comparison of these extreme circulation states can be made by reference to figure 9, which shows the 700-mb. zonal wind speed profiles for the two periods. The sharply peaked profile associated with high index is in marked contrast to the double peaked profile and displaced westerlies with low index.

4. WEATHER IN THE UNITED STATES

TEMPERATURE

Temperatures in the United States during March 1961 averaged warmer than normal over all but the extreme Northeast, the interior valleys of the Pacific Coast States, and Alaska (fig. 1). Greatest positive departures were observed in the Northern Plains and Upper Mississippi Valley—as much as +10° F. in the eastern portions of Montana and North Dakota. Persistence of the temperature pattern, usually considered in terms of the total zero-plus-one-class change [4], was extremely high from February to March, as 93 percent of the country did not change by more than one class (out of five). This compares with an average of 68 percent for the period 1942–60.

The mild temperature regime was quite well related to the mean circulation patterns. At 700 mb. the anomalous flow between the east coast ridge and the southwestern trough was predominantly southeasterly over all but the Far Southwest and Northeast, where northerly flow was associated with cooler conditions (fig. 2). Moreover, strong Pacific westerlies (fig. 4) combined with a deep trough in the Gulf of Alaska and southerly anomalous flow in western Canada (fig. 2) to result in relatively mild Pacific air masses throughout most of the Nation. The thickness in the layer from 1000 to 700 mb. also corresponded well with the temperature pattern (figs. 1, 10).

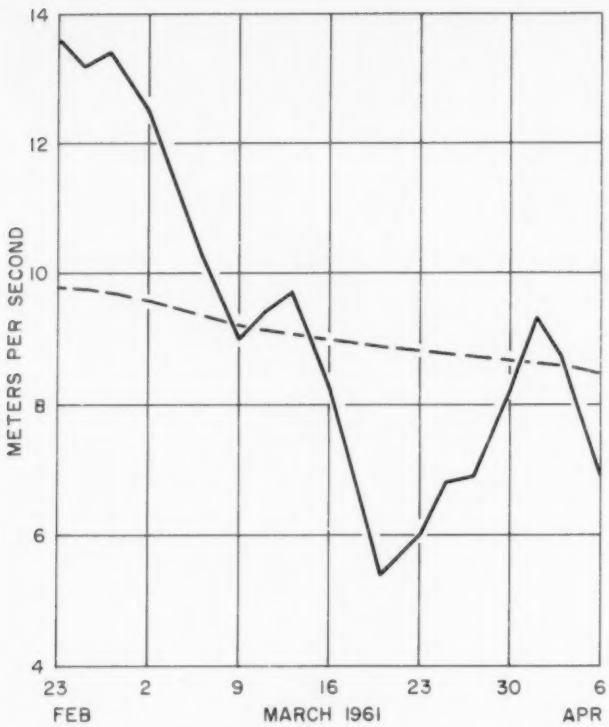

FIGURE 5.—Time variation of speed of 700-mb. westerlies averaged over the western half of the Northern Hemisphere between latitudes 35° and 55° N. Solid line connects 5-day mean zonal index values (plotted at middle of period and computed thrice weekly), while dashed line gives the corresponding "normal" averaged from maps of [6]. Note pronounced index cycle during March.

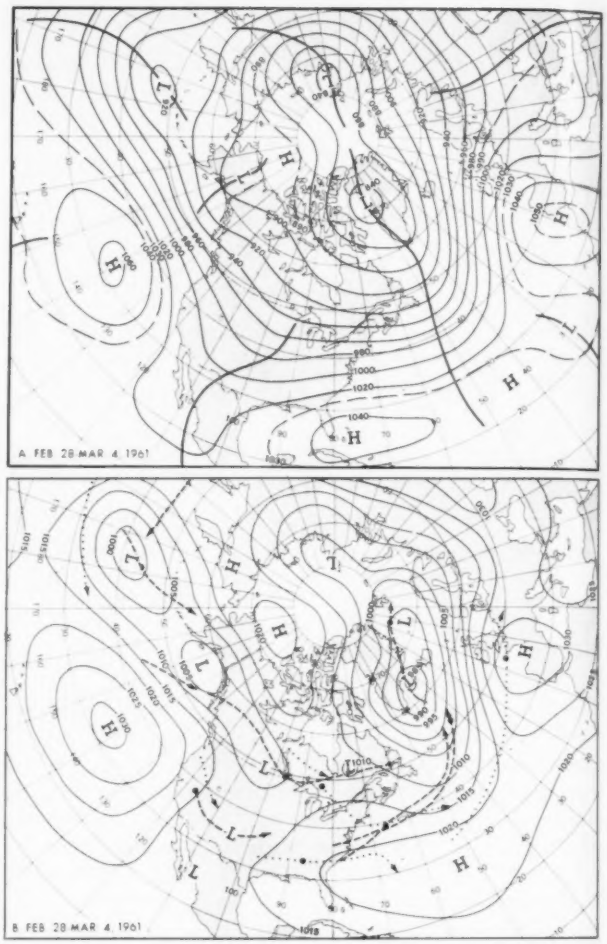

FIGURE 7.—Five-day mean charts for February 28–March 4, 1961 for (A) 700-mb. contours (tens of feet) and (B) sea level isobars (millibars). Tracks of important migratory cyclones (dashed) and anticyclones (dotted), with March 2 positions indicated by large dots, are shown on (B). These circulation patterns were associated with high-index conditions early in the month.

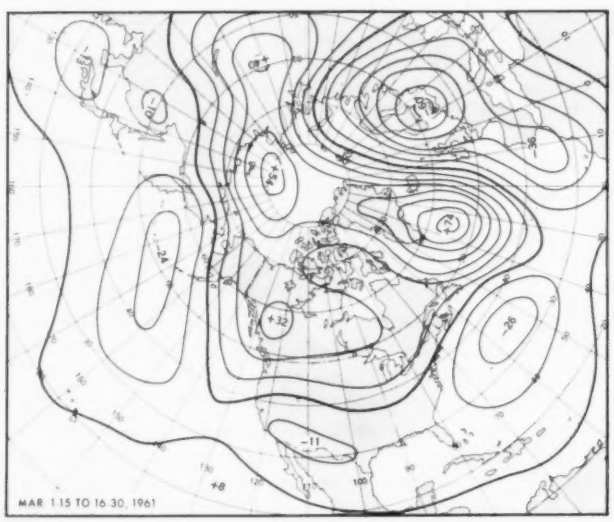

FIGURE 6.—Change of mean 700-mb. height (tens of feet) from first to second half of March 1961. Height rises at higher latitudes and falls at lower latitudes over the Atlantic and North America reflect retrogression of blocking.

A good example of the effect of cloudiness and precipitation on the temperature pattern was observed during March in the Plains States. This is seen by comparing figures 1 and 11. Unusually dry conditions and abundant sunshine were related to the large positive temperature departures in the Northern Plains, while to the south heavy precipitation, much of which was in the form of frequent snows, was associated with temperatures close to normal.

The most unusual warmth occurred during the period March 4 to 6 in the eastern half of the Nation, when early-season maximum temperature records were either established or equaled at Peoria, Ill., Augusta, Ga., Wilmington, N.C., and Richmond, Va. This warmth occurred when the mean ridge over the east coast (fig. 2) reached its greatest strength.

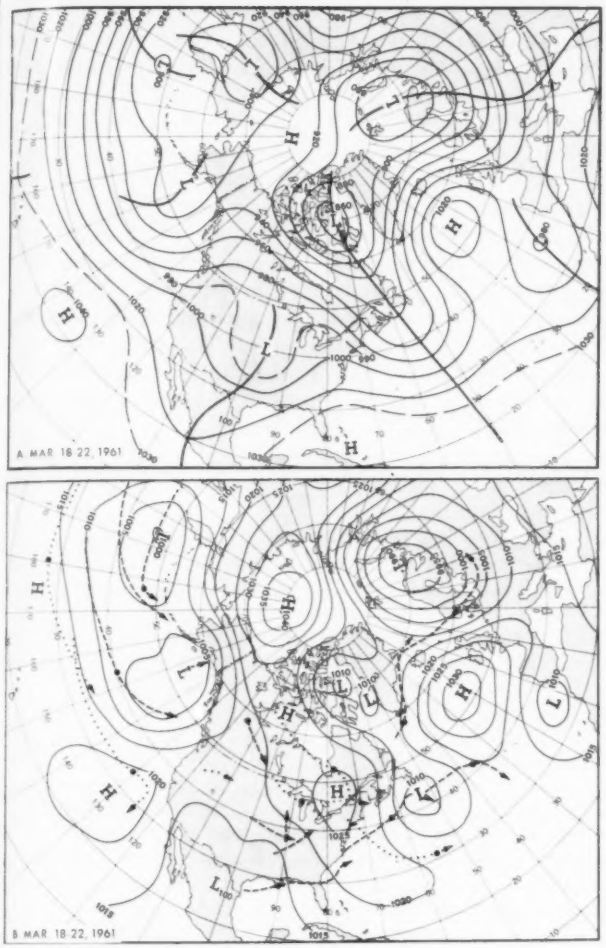

FIGURE 8.—Five-day mean charts, (A) 700 mb. and (B) sea level, for the period March 18–22, 1961, with March 20 positions of cyclones and anticyclones shown by large dots. These circulation patterns were characteristic of low-index conditions late in the month.

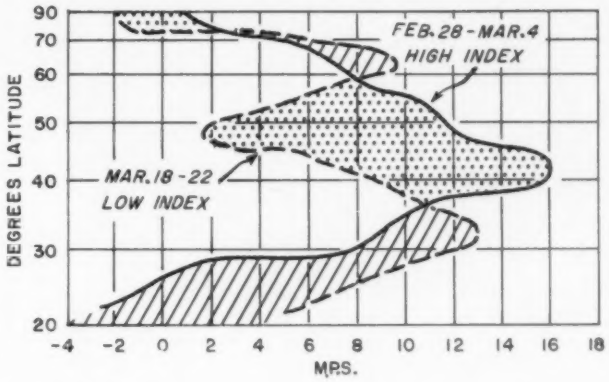

FIGURE 9.—Five-day mean wind speed profiles for high- and low-index stages of the index cycle during March 1961. Decrease in speed of the westerlies at middle latitudes was compensated for by an increase at lower latitudes, thereby tending to conserve the total westerly momentum.

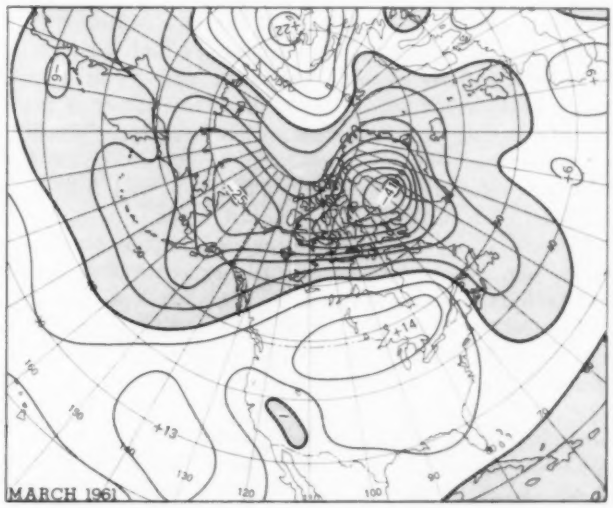

FIGURE 10.—Mean 1,000–700 mb. thickness departures from normal (tens of feet) for March 1961, with areas of subnormal values shaded. Abnormally cold air covered the higher latitudes of North America, but warm conditions were dominant elsewhere over the continent.

Near the end of the month retrogression of blocking into Canada, along with below normal upper-level heights in most of the United States, was accompanied by a gradual change from a warm to a cold regime.

While the contiguous United States had mild weather, Alaska experienced an unusually cold March in all but the southeastern coastal area (fig. 1). A partial explanation for this extreme cold lies in the stronger than normal northeasterly flow from the Arctic Basin at sea level (fig. 3), along with below normal 700-mb. heights (fig. 2). In addition, the thickness in the layer from 1000 to 700 mb. (fig. 10) was well below normal. Note also the unusual extent of the area of cold thickness at higher latitudes, with a center of extreme cold over the Davis Strait and a strong gradient to the south.

PRECIPITATION

Precipitation over much of the Nation was adequate during March, and more than twice the normal amount fell in portions of the Pacific Northwest and the Central Plains (fig. 11). At Yakima, Wash., this was the second wettest March of record, precipitation being more than four times the normal. Near record amounts also fell elsewhere in Washington and Oregon. This heavy precipitation was related to frequent storms moving eastward from the Pacific in faster than normal southwesterly flow (figs. 2, 3, 4).

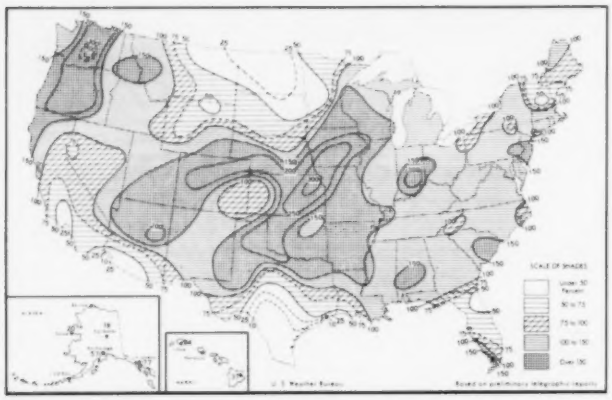

FIGURE 11.—Percentage of normal precipitation for March 1961 (from [5]). Near record amounts of precipitation fell in the Central Plains and Pacific Northwest.

Heavy amounts also fell in the middle of the Nation where Des Moines, Iowa and Kansas City, Mo. both reported record precipitation totals for any March. This resulted in considerable flooding in Iowa and portions of Minnesota and Wisconsin. Record high river stages were reached late in the month along the Cedar River in Iowa at Charles City and Waterloo. This heavy precipitation was associated with the deep mean trough in the Southwest and related storm systems which moved from the southern Plateau to the Great Lakes region.

Unusually dry conditions prevailed in the Northern Plains (fig. 11), where near record dryness was observed in North Dakota. This area lay between two primary storm tracks, one to the south and the other across southern Canada. Ridge conditions and northwesterly flow aloft (fig. 2) also were related to the dryness.

Precipitation was also well below normal in southern portions of California, Arizona, and Texas (fig. 11). At Prescott, Ariz., the period from November 1960 to March 24, 1961 was the driest such period on record since 1865. Near the end of the month, however, a record 24-hour snowfall of 9 inches broke the long dry spell. The dryness in California and Arizona was related to stronger than normal northerly flow in the rear of the mean trough (fig. 2). The precipitation deficit in southern Texas is more difficult to relate to the mean circulation patterns at sea level (fig. 3) and 700 mb. (fig. 2). However, a possible explanation lies in the position of the 700-mb. mean jet maximum through central Texas (fig. 4A), with relatively heavy amounts of precipitation observed north of the jet and light amounts in subsidence and anticyclonic vorticity to its south.

REFERENCES

1. L. P. Stark, "The Weather and Circulation of February 1961—An Example of Attenuation in the Long-Wave Pattern," *Monthly Weather Review*, vol. 89, No. 5, May 1961, pp. 178–184.
2. C. R. Dunn, "The Weather and Circulation of March 1960—A Cold, Snowy Month," *Monthly Weather Review*, vol. 88, No. 3, Mar. 1960, pp. 112–120.
3. J. Namias, "The Index Cycle and Its Role in the General Circulation," *Journal of Meteorology*, vol. 7, No. 2, Apr. 1950, pp. 130–139.
4. J. Namias, "The Annual Course of Month-to-Month Persistence in Climatic Anomalies," *Bulletin of the American Meteorological Society*, vol. 33, No. 7, Sept. 1952, pp. 279–285.
5. U.S. Weather Bureau, *Weekly Weather and Crop Bulletin, National Summary*, vol. XLVIII, No. 14, Apr. 3, 1961.
6. U.S. Weather Bureau, "Normal Weather Charts for the Northern Hemisphere," *Technical Paper* No. 21, Washington, D.C., 1952.

U.S. GOVERNMENT PRINTING OFFICE: 1961